Biochemical and Biophysical Research Communications 440 (2013) 150–156

Contents lists available at ScienceDirect

Biochemical and Biophysical Research Communications

journal homepage: www.elsevier.com/locate/ybbrc

A class II phosphoinositide 3-kinase plays an indispensable role in hepatitis C virus replication

Tomohiko Maehama [a,*], Masayoshi Fukasawa [a], Tomoko Date [b], Takaji Wakita [b], Kentaro Hanada [a]

[a] Department of Biochemistry and Cell Biology, National Institute of Infectious Diseases, Tokyo 162-8640, Japan
[b] Department of Virology II, National Institute of Infectious Diseases, Tokyo 162-8640, Japan

ARTICLE INFO

Article history:
Received 5 September 2013
Available online 18 September 2013

Keywords:
Phosphoinositide
Phosphoinositide 3-kinase (PI3K)
Hepatitis C virus (HCV)

ABSTRACT

Phosphoinositides function as fundamental signaling molecules and play roles in diverse cellular processes. Certain types of viruses may employ host cell phosphoinositide signaling systems to facilitate their replication cycles. Here we demonstrate that the β isoform of class II PI3K (PI3K-C2β) plays an indispensable role in hepatitis C virus (HCV) propagation in human hepatocellular carcinoma cells. Knockdown of PI3K-C2β abrogated HCV propagation in the cell. Using an HCV replicon system, we found that knockdown of PI3K-C2β substantially repressed the full-genome replication, while showing relatively small reductions in sub-genome replication, in which structural proteins including core protein were deleted. We also found that HCV core protein showed the binding activity towards D4-phosphorylated phosphoinositides and overlapped localization with phosphatidylinositol 3,4-bisphosphate in the cell. These results suggest that the phosphoinositide generated by PI3K-C2β plays an indispensable role in the HCV replication cycle through the binding to HCV core protein.

1. Introduction

Phosphoinositides (PIs) are lipid molecules that play crucial roles in diverse cellular functions [1]. In most cases, PIs generated in response to specific stimuli recruit their binding proteins to certain intracellular sites where these proteins exert their functions [2]. Accumulating evidence has identified a number of PI-binding proteins and their functions in fundamental cellular activities, such as cell proliferation, cell growth, vesicle trafficking, and cytoskeletal reorganization [1,2]. PI species are interconverted through phosphorylation and dephosphorylation by a set of specific PI kinases and PI phosphatases. For example, phosphatidylinositol 4-phosphate (PtdIns(4)*P*) is phosphorylated by phosphatidylinositol phosphate 5-kinases to produce phosphatidylinositol 4,5-bisphosphate (PtdIns(4,5)P_2), which is further phosphorylated by class I PI 3-kinases (PI3Ks) to produce phosphatidylinositol 3,4,5-trisphosphate (PtdIns(3,4,5)P_3). This PtdIns(4)*P*–PtdIns(4,5)P_2–PtdIns(3,4,5)P_3 axis is well characterized in its regulation and physiological functions. PtdIns(4)*P* binds to the pleckstrin homology (PH) domain of certain proteins to regulate the intracellular trafficking of proteins and lipids. PtdIns(4,5)P_2 plays a role in regulating cytoskeletal reorganization through the binding to several actin-binding proteins, while PtdIns(3,4,5)P_3 governs cell proliferation and survival through the binding to a set of PH-domain proteins, such as the protein kinase AKT.

Hepatitis C virus (HCV) is an RNA virus that propagates in human hepatic cells and becomes a causative agent for several hepatic disorders, such as steatosis, fibrosis, and hepatocellular carcinomas [3]. HCV is an enveloped virus, of which the viral nucleocapsid is comprised of one type of protein, the core protein. An accumulating body of evidence suggests that the core protein affects diverse host cell function, including proliferation, apoptosis, and metabolism [4], although underlying molecular mechanism of how the core protein acts on these cellular processes remains largely undefined. HCV enters into cells via clathrin-mediated endocytosis, replicates on certain endomembrane structures, and exits from cells using the lipoprotein secretion system [5–7]. These observations clearly show that HCV employs fundamental host cell functions, including cytoskeletal reorganization and intracellular trafficking systems, to facilitate its replication, thereby suggesting that multiple PIs may participate in the HCV replication cycle. Indeed, several studies have demonstrated that type III phosphatidylinositol 4-kinases (PI4K-IIIα and PI4K-IIIβ), which produce PtdIns(4)*P*, are required for HCV replication in HuH-7 hepatocellular carcinoma cells [8–12]. It has been also reported that PI4K-IIIα binds to the HCV nonstructural NS5A protein and participates in the replication complex formation [13–15]. In addition, NS5A

* Corresponding author. Address: Department of Biochemistry and Cell Biology, National Institute of Infectious Diseases, 1-23-1 Toyama, Shinjuku-ku, Tokyo 162-8640, Japan. Fax: +81 3 5285 1157.
E-mail address: tmaehama@nih.go.jp (T. Maehama).

0006-291X/$ - see front matter © 2013 Elsevier Inc. All rights reserved.
http://dx.doi.org/10.1016/j.bbrc.2013.09.048

protein is known to activate class I PI3K and increase survival signals [16,17]. However, participation of other PIs and their metabolizing enzymes in the HCV replication cycle remains largely unknown.

In this study, we show that the β isoform of class II PI3K (PI3K-C2β), a potential phosphatidylinositol 3,4-bisphosphate (PtdIns(3,4)P_2)- and phosphatidylinositol 3-phosphate (PtdIns(3)P)-producing enzyme, is required for the HCV genome replication process. We also demonstrate that PtdIns(3,4)P_2 directly binds to HCV core protein *in vitro* and, in HCV-replicating cells, localizes at endomembrane structures with the core protein. Our study is the first report to demonstrate the requirement of PI3K-C2β for the HCV replication cycle.

2. Materials and methods

2.1. HCV replication assay

Replicon RNAs (SGR, SGR-GND, FGR, and FGR-GND) were prepared from pSGR-JFH1/luc, pSGR-JFH1(GND)/luc, pFGR-JFH1/luc, and pFGR-JFH1(GND)/luc as described previously [18,19]. HuH-7.5.1-8 cells on 48-well plates were transfected with one of the replicon RNAs as described above and then cultured for 22–72 h. Luciferase activity was determined using the Luciferase Assay System (Promega) according to the manufacturer's protocol.

2.2. Lipid binding assay

In order to prepare liposomes, egg phosphatidylcholine (500 μg, Avanti Polar Lipids) and *sn*-1-palmitoy-2-oleoylphosphatidylethanolamine (125 μg, Sigma–Aldrich) along with 3 μg each of PtdIns(3)P, PtdIns(4)P, phosphatidylinositol 5-phosphate, PtdIns(3,4)P_2, PtdIns(4,5)P_2, or PtdIns(3,4,5)P_3 were dried under vacuum. All PIs used in this study were in the dipalmitoylated form and obtained from Cayman. The dried lipids were resuspended in 100 μl of resuspension buffer (50 mM 3-morpholinopropanesulfonic acid–NaOH [pH 7.2], 100 mM NaCl, and 1 mM DTT) and incubated at 65 °C for 1 h. The liposomes were then frozen in liquid nitrogen and thawed at 37 °C for three cycles. The liposome binding assay was performed in a solution containing 100 μl of liposome solution and 2 μl of fraction-17 (of Sephacryl S-300 column chromatography) containing recombinant core protein. After incubation at 4 °C for 1 h, liposomes were collected by centrifugation at 20,000*g* for 20 min, and core protein precipitated with liposomes

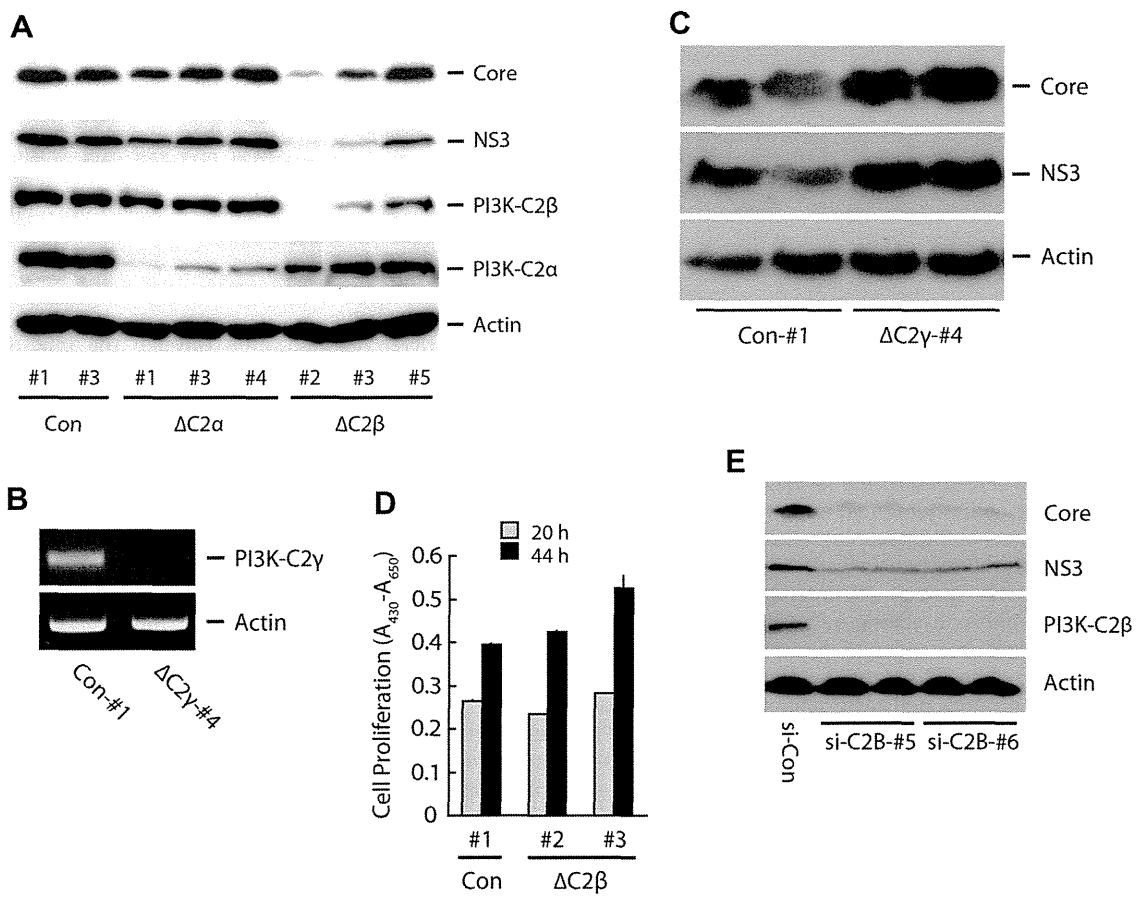

Fig. 1. PI3K-C2β is indispensable for HCV propagation in HuH-7.5.1-8 cells. (A) Control (Con-#1 and #3), PI3K-C2α-knockdown (ΔC2α-#1, #3, and #4), and PI3K-C2β-knockdown (ΔC2β-#2, #3, and #5) cells were infected with HCV. After a 5-day culture, viral proteins (core and NS3) accumulated in cells were detected by immunoblotting. Expression of PI3K-C2α and PI3K-C2β along with actin (as a loading control) was also represented. (B) RNA fractions from Control (Con-#1) and PI3K-C2γ-knockdown (ΔC2γ-#4) cells were subjected to RT-PCR analysis to detect PI3K-C2γ and actin mRNAs. RNA extraction and RT-PCR were conducted as described under Section 2 (HCV entry assay section). (C) Control (Con-#1) and PI3K-C2γ-knockdown (ΔC2γ-#4) cells were infected with HCV. After a 5-day culture, viral proteins (core and NS3) accumulated in the cells were detected by immunoblotting. (D) In order to determine the proliferation of control (Con-#1) and PI3K-C2β-knockdown (ΔC2β-#2 and #3) cells, 2.5×10^3 cells were plated on 96-well plates and cultured for the indicated times. Proliferation was determined as described under Section 2. Data are represented as the mean ± SD from quadruplicated experiments. (E) HuH-7.5.1-8 cells were transfected with indicated siRNAs (si-Con, si-C2B-#5, and si-C2B-#6) twice with a 3-day interval. Cells were then infected with HCV. After a 5-day culture, viral proteins (core and NS3) accumulated in the cells were detected by immunoblotting. Expression of PI3K-C2β along with actin (as a loading control) was also represented. Typical data from three independent experiments are presented (A, C, E).

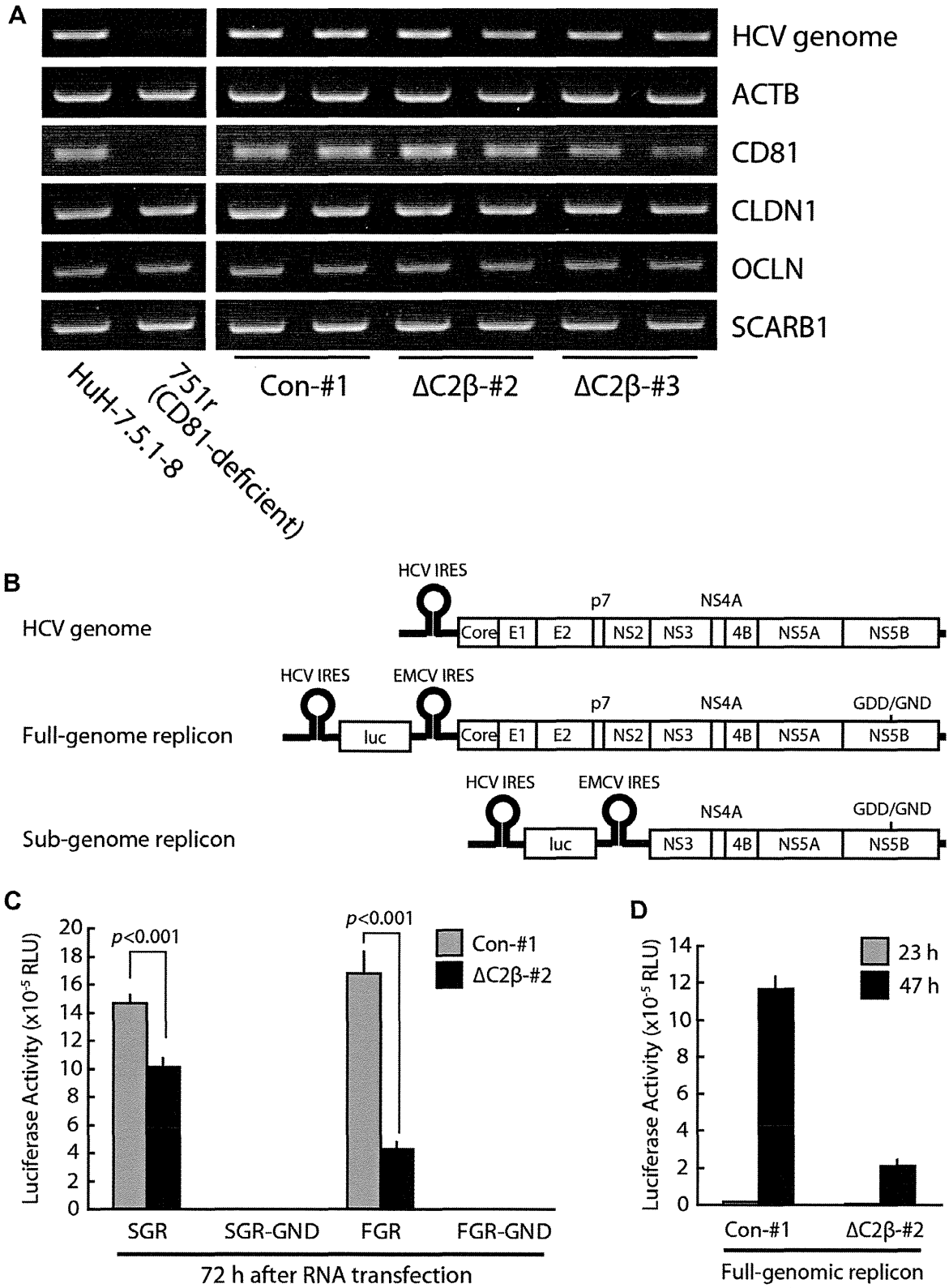

Fig. 2. PI3K-C2β knockdown represses HCV replication. (A) PI3K-C2β knockdown does not affect HCV entry. Control (Con-#1) and PI3K-C2β-knockdown (ΔC2β-#2 and #3) cells as well as HuH-7.5.1-8 (as a positive control) and CD81-deficient 751r (as a negative control) cells were subjected to HCV entry assay described under Section 2. Experiments were performed in duplicate (except positive and negative controls) and typical images from repeated experiments are presented. (B) Schematic diagram of HCV genomic and replicon RNA. (C) Control (Con-#1, gray column) and PI3K-C2β-knockdown (ΔC2β-#2, filled column) cells were transfected with RNA from either the sub-genomic replicon (SGR), replication-defective SGR (SGR-GND), full-genomic replicon (FGR), or replication-defective FGR (FGR-GND). After a 72-h culture, the luciferase activity of each sample was determined as described in Section 2. Data are represented as the mean ± SD from triplicated experiments. An unpaired Student's *t*-test was used to calculate statistical significance. (D) Control (Con-#1) and PI3K-C2β-knockdown (ΔC2β-#2) cells were transfected with the full-genomic replicon RNA. After the indicated time of culture, the luciferase activity of each sample was determined and represented as described above.

was analyzed by immunoblot analysis. The relative intensities of immunoreactive core protein bands were measured using the ImageJ Java applet.

2.3. HCV entry assay

Cells (1.4×10^5) were plated onto a well of a 12-well plate and cultured for 1 day. After removal of the medium, 0.35 ml of HCV-containing culture medium were added onto the cells and incubated for 2 h at 37 °C. Then, the medium was changed to normal growth medium supplemented by 0.1% Pluronic F-68 (Invitrogen). After the incubation at 37 °C for 2 h, the cells were rinsed with PBS containing 0.1% Pluronic F-68, followed by the incubation in 0.5 ml of AccuMax (Innovative Cell Technologies) for 5 min at room temperature in order to detach cells from the vessel and remove bound viruses but not internalized viruses [20]. The cells were then collected by centrifugation, and RNA was extracted using TRIzol Reagent (Invitrogen). The RNA fractions were transcribed into cDNA using Moloney murine leukemia virus reverse transcriptase (Takara), followed by PCR analyses. In order to analyze the level of HCV genome RNA and transcripts for host cell factors, PCR was conducted in a 10-μl reaction mixture using 20 ng of cDNA as a template and Platinum PCR Super Mix (Invitrogen) according to the manufacturer's protocol. Primers used in this study were listed in Supplementary Table S1.

2.4. Supplementary methods

For cell culture, transfection, DNA construction, recombinant core protein preparation, immunoblot analysis, immunofluorescent assay and HCV infection, please consult Supplementary Data.

3. Results and discussion

3.1. PI3K-C2β is indispensable for HCV propagation in cells

Class II PI3Ks, that are relatively insensitive towards wortmannin, catalyze phosphorylation of PtdIns and PtdIns(4)*P* to produce PtdIns(3)*P* and PtdIns(3,4)P_2, respectively. Biological processes potentially controlled by these PIs (PtdIns(3)*P* for endocytosis; PtdIns(3,4)P_2 for endocytosis and proliferation) may affect HCV propagation [1,21]. In the human genome, there are three isoforms of class II PI3K, PI3K-C2α, PI3K-C2β, and PI3K-C2γ. The expression of all isoforms in HuH-7.5.1-8 cell was detected by immunoblot analysis (see Fig. 1A) and reverse transcription-polymerase chain reaction (RT-PCR) (Fig. 1B and data not shown). Thus, we performed short hairpin RNA (shRNA)-mediated gene silencing of PI3K-C2α, PI3K-C2β, and PI3K-C2γ in HuH-7.5.1-8 cell to test their contribution to HCV propagation in the cell. We established multiple stable clones (ΔC2α-#1, #3, and #4; ΔC2β-#2, #3, and #5; ΔC2γ-#4) in which the expression of PI3K-C2α, PI3K-C2β, or PI3K-C2γ was reduced to various extents (see Fig. 1A and B) as well as stable clones harboring control constructs (Con-#1 and #3). These cells were infected with cell-cultured HCV (JFH1 strain) and incubated for 5 days to allow the virus propagation. As shown in Fig. 1A, while HCV core and NS3 proteins were accumulated in control cells, the accumulation of these viral proteins was greatly reduced in PI3K-C2β-knockdown cells. Quite severe reduction in HCV protein accumulation was observed in ΔC2β-#2, in which PI3K-C2β expression was almost undetectable; while ΔC2β-#3 and ΔC2β-#5, in which PI3K-C2β expression was modestly inhibited, showed partial reduction in HCV protein accumulation (Fig. 1A). This result suggests a dose-dependent requirement of PI3K-C2β in HCV propagation in the cell. In contrast, the effect of PI3K-C2α knockdown on viral protein accumulation was limited, although PI3K-C2α expression was almost undetectable in the cell (see ΔC2α-#1, Fig. 1A). In addition, the depletion of PI3K-C2γ (ΔC2γ-#4), as estimated by RT-PCR (Fig. 1B), did not affect viral protein accumulation (Fig. 1C). Thus we focused on PI3K-C2β functions in HCV propagation using ΔC2β-#2 and ΔC2β-#3 cells for further analyses, because these cell lines showed significant decreases in viral protein accumulation at 5 days after the infection (Fig. 1A). It should be noted that these PI3K-C2α-, PI3K-C2β-, and PI3K-C2γ-knockdown cells did not show decreased proliferation (Fig. 1D and data not shown). Further the introduction of PI3K-C2β-directed small interfering RNAs (siRNAs) (si-C2B-#5 and si-C2B-#6) into HuH-7.5.1-8 cells induced significant reduction of PI3K-C2β expression and resulted in decreases in viral protein accumulation at 5 days after the infection when compared to control cell (Fig. 1E). These non-coding small RNAs (si-C2B-#5, si-C2B-#6, and PIK3C2B-SH) target distinct sequences of PI3K-C2β mRNA, excluding the possibility that the inhibitory effect of PI3K-C2β knockdown on HCV propagation was due to the off-target effect. In addition, as shown in Fig. S1, the expression of mouse PI3K-C2β restored HCV propagation, that was repressed in PI3K-C2β-knockdown cell. We also tested virus release from PI3K-C2β-depleted cells and found that, as reflecting the reduction of HCV protein accumulation in cells (Fig. 1A), culture supernatant from HCV-infected ΔC2β-#2 and ΔC2β-#3 cells showed reduced infectivity towards naïve HuH-7.5.1-8 cells (Fig. S2). These observations taken together suggest that PI3K-C2β plays an indispensable role in HCV propagation in cells.

3.2. PI3K-C2β plays a role in HCV genome replication process

Both of PI3K-C2β-produced PIs, PtdIns(3)*P* and PtdIns(3,4)P_2, are implicated in endocytosis, the cellular process which HCV

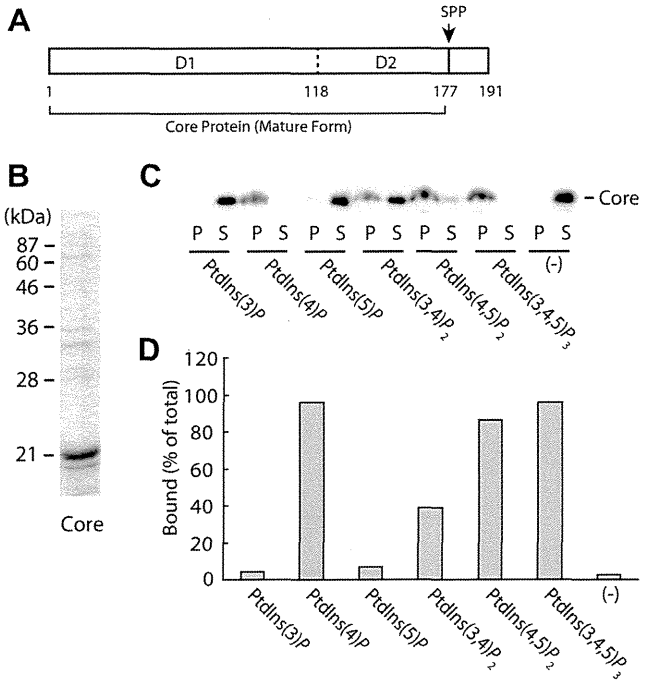

Fig. 3. HCV core protein binds to phosphoinositides *in vitro*. (A) Schematic diagram of HCV core protein. SPP, signal peptide peptidase. (B) Coomassie brilliant blue staining of recombinant core protein prepared by Sephacryl S-300 column chromatography (fraction-17). (C) Recombinant core protein bound to liposomes containing indicated PIs (P) and left unbound (S) were detected by immunoblot analysis. (D) Quantification of the bound core protein against the total amount shown in (C). Typical data from two independent experiments are presented.

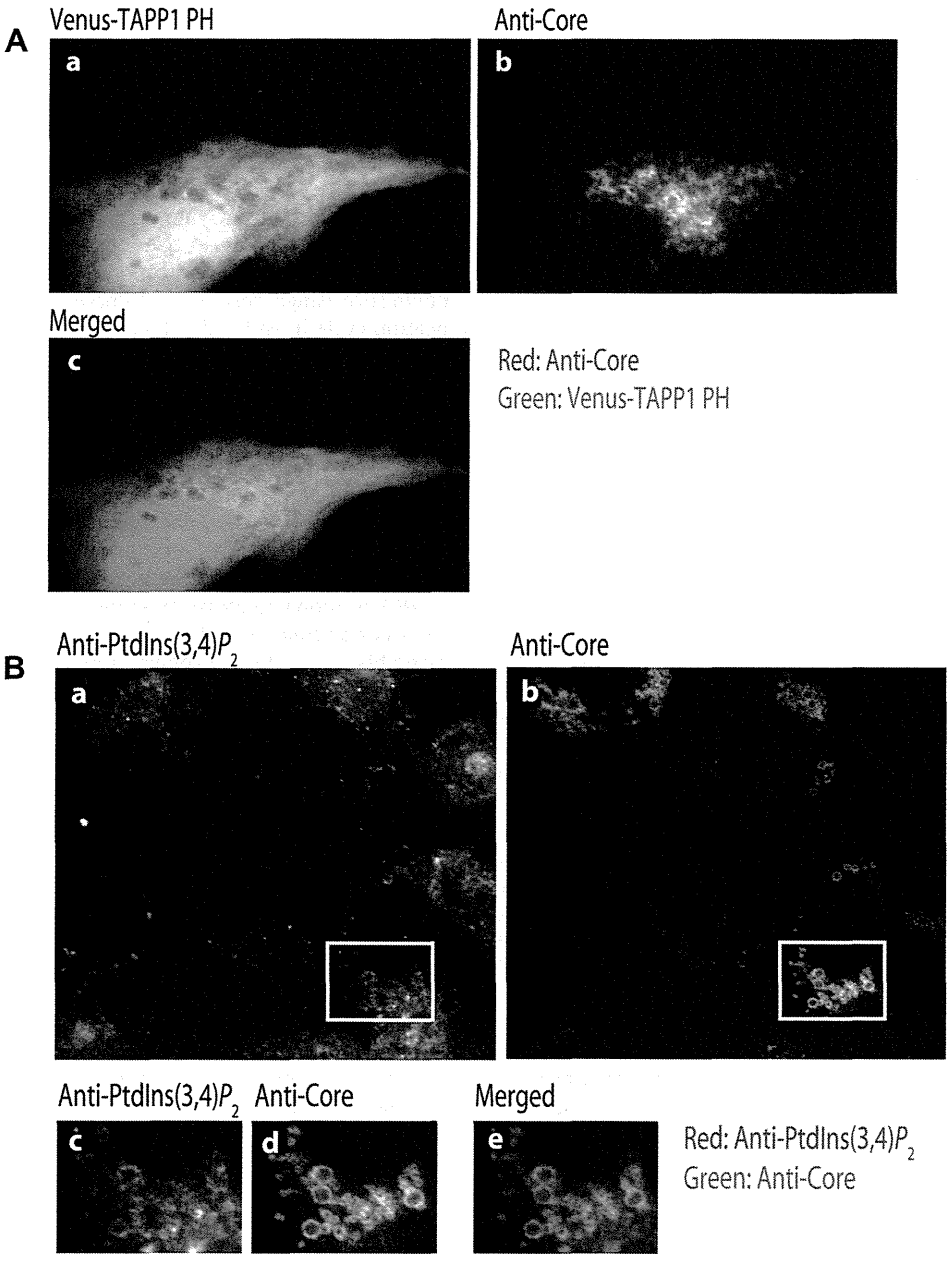

Fig. 4. PtdIns(3,4)P_2 accumulates in endomembrane structures with HCV core protein. (A) HuH-7.5.1-8 cells grown on a coverslip were transfected with TAPP1-PH/pVenus and Core-195/pEF1 expression constructs. After 2 days of culture, the cells were probed with anti-GFP (a) and anti-core (b) antibodies. Merged image is shown in (c). (B) HCV-infected HuH-7.5.1-8 cells were probed with anti-PtdIns(3,4)P_2 (a) and anti-core (b) antibodies. The selected area is shown at higher magnification in (c and d), and the merged image is shown in (e). Typical images from repeated experiments are presented.

employs to enter into the cell. Thus we first tested whether viral entry was affected by PI3K-C2β knockdown. Cells (ΔC2β-#2, ΔC2β-#3 and Con-#1) were exposed to HCV, followed by the incubation for additional 2 h to allow the virus enter into the cell. Then internalized HCV was detected by RT-PCR analysis. As shown in Fig. 2A, HCV genome RNA was detected in both PI3K-C2β-knockdown cells (ΔC2β-#2 and ΔC2β-#3) as well as control cell (Con-#1) and parental HuH-7.5.1-8 cell; while the depletion of CD81, a critical receptor for HCV, completely abrogated HCV entry (751r). This result suggests that PI3K-C2β did not contribute to entry step of HCV. It is also of note that the expression of cell surface molecules (CD81, CLDN1, OCLN, and SCARB1) that are involved in HCV entry was not affected by PI3K-C2β knockdown (Fig. 2A).

This result, together with the result shown in Fig. 1, prompts us that PI3K-C2β primarily affects intracellular HCV propagation step(s) such as genome replication process. We therefore tested the requirement of PI3K-C2β for HCV genome replication using HCV replicon systems. We used full-genomic and sub-genomic replicon systems that employ firefly luciferase as the reporter. The full-genomic replicon possesses structural proteins including core (Fig. 2B), and cells harboring the replicon potentially release infectious virus into the medium. Conversely, the sub-genomic replicon lacks structural proteins in addition to p7 and NS2 proteins (Fig. 2B). Cells were transfected with these replicon RNAs, and replication activity was determined by measuring luciferase activity. As shown in Fig. 2C, ΔC2β-#2 showed reduced replication activity of both sub-genomic (Fig. 2C, SGR) and full-genomic (Fig. 2C, FGR) replicons compared to their replication activity in control cell (Con-#1) at 72 h after the transfection. Replication-deficient mutants SGR-GND and FGR-GND exhibited no replication

activities under this condition (Fig. 2C). The transfection efficiencies of Con-#1 and ΔC2β-#2 cells were almost comparable under these conditions (data not shown). We did not use ΔC2β-#3 cell for this assay, because this cell line did not show comparable transfection efficiency for replicon RNAs (data not shown). Intriguingly, the inhibitory effect of PI3K-C2β knockdown was much larger in the full-genomic replicon system (75% reduction) than in the sub-genomic replicon system (31% reduction) (Fig. 2C). In addition, a similar magnitude of inhibition (78% reduction) was also observed in cells 47 h after the transfection of the full-genomic replicon RNA (Fig. 2D); at that time point, infectious particles for the reinfection were not sufficiently released into the culture medium. These results suggest that full genome-specific elements, including core protein, E1/E2 envelope proteins, p7 protein, and NS2 protein (Fig. 2B), were affected by PI3K-C2β itself and/or PIs generated by PI3K-C2β and involved in the replication process.

3.3. HCV core protein binds to PtdIns(3,4)P_2

HCV core protein encompasses the the D1 region (basic domain) and the D2 region (hydrophobic domain) (Fig. 3A), suggesting the interaction of the core protein with negatively charged lipids, such as PIs. Therefore we next focused on the core protein and attempted to test the binding of the core protein toward PIs. Although we have difficulties in preparing full-length core protein, recombinant core protein, encompassing the D1 region but not the D2 region was successfully produced in *Escherichia coli* (Fig. 3B), and then subjected to a liposome binding assay. As shown in Fig. 3C and D, the core protein showed binding activity toward D4-phosphorylated PIs (PtdIns(4)*P*, PtdIns(3,4)P_2, PtdIns(4,5)P_2, and PtdIns(3,4,5)P_3) *in vitro*. It should be noted that recombinant core protein used for the *in vitro* binding assay lacks D2 region, thus the *in vitro* binding profile does not necessarily reflect *in vivo* function. Therefore, we next tested the localization of these D4-phosphorylated PIs with HCV core protein in cells and found overlapped localization of PtdIns(3,4)P_2 and HCV core protein in HCV-infected HuH-7.5.1-8 cells. In HuH-7.5.1-8 cells TAPP1 PH domain, a widely used PtdIns(3,4)P_2–selective probe [22], showed reticular staining pattern, which appeared to partially overlap with HCV core protein (Fig. 4A); although the overlapped staining was not so clear presumably due to relatively low binding affinity of the PH domain towards PtdIns(3,4)P_2 [23] and high background cytoplasmic staining. Therefore we next used an anti-PtdIns(3,4)P_2 antibody [24] to detect PtdIns(3,4)P_2 in HCV-infected HuH-7.5.1-8 cells. The anti-PtdIns(3,4)P_2 antibody showed, in addition to reticular staining pattern, staining of ring-like intracellular structures, which overlapped with the core protein (Fig. 4B). It is of note that other PIs, including PtdIns(4)*P*, did not show significant overlapped staining with the core protein (see Fig. S3 and data not shown). Although we are still unable to sufficiently explain why the core protein selectively associated with PtdIns(3,4)P_2 but not with other core-binding PIs in cells; these results suggest that PtdIns(3,4)P_2 accumulated in endomembrane structures through direct binding to HCV core protein.

3.4. Participation of PIs in the HCV replication cycle

The results obtained in this study show that PI3K-C2β plays an indispensable role in HCV replication in cells presumably through the production of PtdIns(3,4)P_2. Previous studies have demonstrated that PI4Ks are essential for HCV replication in cells through the interaction with NS5A protein to facilitate replication complex formation [13]. Our results raise the possibility that, in addition to playing a direct role in the replication complex formation, PI4Ks function as producers of PtdIns(4)*P*, a precursor of PtdIns(3,4)P_2. PtdIns(3,4)P_2, produced by PI3K-C2β, might play a role in the replication process reciprocally with PtdIns(4)*P*, although the precise action of PtdIns(3,4)P_2 remains elusive.

PtdIns(3,4)P_2 can be dephosphorylated by inositol polyphosphate 4-phosphatases (INPP4A and INPP4B) and potentially by PTEN to produce PtdIns(3)*P* and PtdIns(4)*P*, respectively. Knockdown of INPP4A did not affect HCV protein accumulation in cells (Fig. S4). The expression of INPP4B was not detected in HuH-7.5.1-8 cells (data not shown). These results suggest that PTEN plays a dominant role in the breakdown of PtdIns(3,4)P_2, which is required for the HCV replication cycle. Nonetheless, PTEN knockdown surprisingly resulted in complete abrogation of the HCV replication cycle in HuH-7.5.1-8 cells, although cell viability was not affected by the knockdown (Fig. S4 and data not shown). Although we can not exclude the possibility that PtdIns(3,4)P_2 is catabolized by unidentified enzyme(s); it is more likely that PTEN knockdown may increase multiple PI species, such as PtdIns(3)*P* and PtdIns(3,4,5)P_3 in addition to PtdIns(3,4)P_2, thereby disrupting a wide range of PI-regulated signals and resulting in unexpected abrogation of the HCV replication cycle. This observation suggests that multiple PIs, in addition to PtdIns(4)*P* [8–13,25] and PtdIns(3,4)P_2 (this study), are involved in the HCV replication cycle.

HCV is known to utilize endomembrane structures derived from the endoplasmic reticulum for the sites of its replication and assembly [5,7]; lipid droplets function as crucial intracellular organelles for HCV replication and assembly. HCV JFH1 core protein predominantly localizes near lipid droplets, showing a "ring"-like shape [26]. Crucial role of PI3K-C2β, as observed in Figs. 1A and 2C, prompted us to test whether PI3K-C2β knockdown affects lipid droplet formation. However, under normal growth condition and even after oleate addition, there was no difference in lipid droplet formation between PI3K-C2β-knockdown cells and control cells (Fig. S5). Furthermore, core protein localization was not altered in PI3K-C2β-knockdown cells as compared to its localization in control cells (Fig. S6). These results suggest that PI3K-C2β may not be involved in lipid droplet formation and that PI3K-C2β may be involved in the process of HCV replication after the recruitment of HCV proteins to the sites near lipid droplets. PtdIns(3,4)P_2 might be produced by PI3K-C2β, presumably at the endoplasmic reticulum, and then recruited to the core protein accumulation site through direct binding with core protein. Although further study will be required to reveal the underlying mechanism by which PIs regulate HCV replication process, results obtained in this study imply that manipulating PI signals may control HCV propagation.

Role of funding sources

This work was supported by Grants-in-Aid for Scientific Research from the Japanese Ministry of Education, Culture, Sports, and Science; and by Grants-in-Aid for Scientific Research and for Cancer Research from the Ministry of Health, Labor, Welfare, and Technology.

Acknowledgment

We are grateful to Dr. Yoshihiro Miwa (University of Tsukuba, Japan) for providing pOSTet vector with Epstein–Barr virus-based episomal replication system.

Appendix A. Supplementary data

Supplementary data associated with this article can be found, in the online version, at http://dx.doi.org/10.1016/j.bbrc.2013.09.048.

References

[1] G. Di Paolo, P. De Camilli, Phosphoinositides in cell regulation and membrane dynamics, Nature 443 (2006) 651–657.

[2] T.G. Kutateladze, Translation of the phosphoinositide code by PI effectors, Nat. Chem. Biol. 6 (2010) 507–513.

[3] M. Levrero, Viral hepatitis and liver cancer: the case of hepatitis C, Oncogene 25 (2006) 3834–3847.

[4] J. Dubuisson, Hepatitis C virus proteins, World J. Gastroenterol. 13 (2007) 2406–2415.

[5] D.M. Jones, J. McLauchlan, Hepatitis C virus: assembly and release of virus particles, J. Biol. Chem. 285 (2010) 22733–22739.

[6] M.A. Joyce, D.L. Tyrrell, The cell biology of hepatitis C virus, Microbes Infect. 12 (2010) 263–271.

[7] K. Ogawa, T. Hishiki, Y. Shimizu, K. Funami, K. Sugiyama, Y. Miyanari, K. Shimotohno, Hepatitis C virus utilizes lipid droplet for production of infectious virus, Proc. Jpn. Acad. Ser. B Phys. Biol. Sci. 85 (2009) 217–228.

[8] K.L. Berger, J.D. Cooper, N.S. Heaton, R. Yoon, T.E. Oakland, T.X. Jordan, G. Mateu, A. Grakoui, G. Randall, Roles for endocytic trafficking and phosphatidylinositol 4-kinase III alpha in hepatitis C virus replication, Proc. Natl. Acad. Sci. USA 106 (2009) 7577–7582.

[9] J. Borawski, P. Troke, X. Puyang, V. Gibaja, S. Zhao, C. Mickanin, J. Leighton-Davies, C.J. Wilson, V. Myer, I. Cornellataracido, J. Baryza, J. Tallarico, G. Joberty, M. Bantscheff, M. Schirle, T. Bouwmeester, J.E. Mathy, K. Lin, T. Compton, M. Labow, B. Wiedmann, L.A. Gaither, Class III phosphatidylinositol 4-kinase alpha and beta are novel host factor regulators of hepatitis C virus replication, J. Virol. 83 (2009) 10058–10074.

[10] A.W. Tai, Y. Benita, L.F. Peng, S.S. Kim, N. Sakamoto, R.J. Xavier, R.T. Chung, A functional genomic screen identifies cellular cofactors of hepatitis C virus replication, Cell Host Microbe 5 (2009) 298–307.

[11] M. Trotard, C. Lepere-Douard, M. Regeard, C. Piquet-Pellorce, D. Lavillette, F.L. Cosset, P. Gripon, J. Le Seyec, Kinases required in hepatitis C virus entry and replication highlighted by small interference RNA screening, FASEB J. 23 (2009) 3780–3789.

[12] F.H. Vaillancourt, L. Pilote, M. Cartier, J. Lippens, M. Liuzzi, R.C. Bethell, M.G. Cordingley, G. Kukolj, Identification of a lipid kinase as a host factor involved in hepatitis C virus RNA replication, Virology 387 (2009) 5–10.

[13] S. Reiss, I. Rebhan, P. Backes, I. Romero-Brey, H. Erfle, P. Matula, L. Kaderali, M. Poenisch, H. Blankenburg, M.S. Hiet, T. Longerich, S. Diehl, F. Ramirez, T. Balla, K. Rohr, A. Kaul, S. Buhler, R. Pepperkok, T. Lengauer, M. Albrecht, R. Eils, P. Schirmacher, V. Lohmann, R. Bartenschlager, Recruitment and activation of a lipid kinase by hepatitis C virus NS5A is essential for integrity of the membranous replication compartment, Cell Host Microbe 9 (2011) 32–45.

[14] Y.S. Lim, S.B. Hwang, Hepatitis C virus NS5A protein interacts with phosphatidylinositol 4-kinase type III alpha and regulates viral propagation, J. Biol. Chem. 286 (2011) 11290–11298.

[15] S. Reiss, C. Harak, I. Romero-Brey, D. Radujkovic, R. Klein, A. Ruggieri, I. Rebhan, R. Bartenschlager, V. Lohmann, The lipid kinase phosphatidylinositol-4 kinase III alpha regulates the phosphorylation status of hepatitis C virus NS5A, PLoS Pathog. 9 (2013) e1003359.

[16] A. Street, A. Macdonald, K. Crowder, M. Harris, The Hepatitis C virus NS5A protein activates a phosphoinositide 3-kinase-dependent survival signaling cascade, J. Biol. Chem. 279 (2004) 12232–12241.

[17] A. Street, A. Macdonald, C. McCormick, M. Harris, Hepatitis C virus NS5A-mediated activation of phosphoinositide 3-kinase results in stabilization of cellular beta-catenin and stimulation of beta-catenin-responsive transcription, J. Virol. 79 (2005) 5006–5016.

[18] M. Miyamoto, T. Kato, T. Date, M. Mizokami, T. Wakita, Comparison between subgenomic replicons of hepatitis C virus genotypes 2a (JFH-1) and 1b (Con1 NK5.1), Intervirology 49 (2006) 37–43.

[19] T. Date, M. Miyamoto, T. Kato, K. Morikawa, A. Murayama, D. Akazawa, J. Tanabe, S. Sone, M. Mizokami, T. Wakita, An infectious and selectable full-length replicon system with hepatitis C virus JFH-1 strain, Hepatol. Res. 37 (2007) 433–443.

[20] Y.Y. Zhang, B.H. Zhang, K. Ishii, T.J. Liang, Novel function of CD81 in controlling hepatitis C virus replication, J. Virol. 84 (2010) 3396–3407.

[21] Y. Posor, M. Eichhorn-Gruenig, D. Puchkov, J. Schoneberg, A. Ullrich, A. Lampe, R. Muller, S. Zarbakhsh, F. Gulluni, E. Hirsch, M. Krauss, C. Schultz, J. Schmoranzer, F. Noe, V. Haucke, Spatiotemporal control of endocytosis by phosphatidylinositol-3,4-bisphosphate, Nature 499 (2013) 233–237.

[22] W.A. Kimber, L. Trinkle-Mulcahy, P.C. Cheung, M. Deak, L.J. Marsden, A. Kieloch, S. Watt, R.T. Javier, A. Gray, C.P. Downes, J.M. Lucocq, D.R. Alessi, Evidence that the tandem-pleckstrin-homology-domain-containing protein TAPP1 interacts with Ptd(3,4)P_2 and the multi-PDZ-domain-containing protein MUPP1 *in vivo*, Biochem. J. 361 (2002) 525–536.

[23] M. Furutani, K. Tsujita, T. Itoh, T. Ijuin, T. Takenawa, Application of phosphoinositide-binding domains for the detection and quantification of specific phosphoinositides, Anal. Biochem. 355 (2006) 8–18.

[24] T. Yokogawa, S. Nagata, Y. Nishio, T. Tsutsumi, S. Ihara, R. Shirai, K. Morita, M. Umeda, Y. Shirai, N. Saitoh, Y. Fukui, Evidence that 3′-phosphorylated polyphosphoinositides are generated at the nuclear surface: use of immunostaining technique with monoclonal antibodies specific for PI 3,4-P(2), FEBS Lett. 473 (2000) 222–226.

[25] B. Bishe, G.H. Syed, S.J. Field, A. Siddiqui, Role of phosphatidylinositol 4-phosphate (PI4P) and its binding protein GOLPH3 in hepatitis C virus secretion, J. Biol. Chem. 287 (2012) 27637–27647.

[26] Y. Miyanari, K. Atsuzawa, N. Usuda, K. Watashi, T. Hishiki, M. Zayas, R. Bartenschlager, T. Wakita, M. Hijikata, K. Shimotohno, The lipid droplet is an important organelle for hepatitis C virus production, Nat. Cell Biol. 9 (2007) 1089–1097.

Biochemical and Biophysical Research Communications 443 (2014) 808–813

Contents lists available at ScienceDirect

Biochemical and Biophysical Research Communications

journal homepage: www.elsevier.com/locate/ybbrc

Evaluation and identification of hepatitis B virus entry inhibitors using HepG2 cells overexpressing a membrane transporter NTCP ☆

Masashi Iwamoto [a,b], Koichi Watashi [a,b,*], Senko Tsukuda [a,c], Hussein Hassan Aly [a], Masayoshi Fukasawa [d], Akira Fujimoto [a], Ryosuke Suzuki [a], Hideki Aizaki [a], Takayoshi Ito [e], Osamu Koiwai [b], Hiroyuki Kusuhara [f], Takaji Wakita [a]

[a] Department of Virology II, National Institute of Infectious Diseases, Tokyo 162-8640, Japan
[b] Department of Applied Biological Science, Tokyo University of Sciences, Noda 278-8510, Japan
[c] Micro-signaling Regulation Technology Unit, RIKEN Center for Life Science Technologies, Wako 351-0198, Japan
[d] Department of Biochemistry and Cell Biology, National Institute of Infectious Diseases, Tokyo 162-8640, Japan
[e] Division of Gastroenterology, Department of Medicine, Showa University School of Medicine, Tokyo 142-8666, Japan
[f] The University of Tokyo, Graduate School of Pharmaceutical Sciences, Tokyo 113-0033, Japan

ARTICLE INFO

Article history:
Received 24 November 2013
Available online 14 December 2013

Keywords:
HBV
Infection
NTCP
DMSO
Cyclosporin
Oxysterol

ABSTRACT

Hepatitis B virus (HBV) entry has been analyzed using infection-susceptible cells, including primary human hepatocytes, primary tupaia hepatocytes, and HepaRG cells. Recently, the sodium taurocholate cotransporting polypeptide (NTCP) membrane transporter was reported as an HBV entry receptor. In this study, we established a strain of HepG2 cells engineered to overexpress the human NTCP gene (HepG2-hNTCP-C4 cells). HepG2-hNTCP-C4 cells were shown to be susceptible to infection by blood-borne and cell culture-derived HBV. HBV infection was facilitated by pretreating cells with 3% dimethyl sulfoxide permitting nearly 50% of the cells to be infected with HBV. Knockdown analysis suggested that HBV infection of HepG2-hNTCP-C4 cells was mediated by NTCP. HBV infection was blocked by an anti-HBV surface protein neutralizing antibody, by compounds known to inhibit NTCP transporter activity, and by cyclosporin A and its derivatives. The infection assay suggested that cyclosporin B was a more potent inhibitor of HBV entry than was cyclosporin A. Further chemical screening identified oxysterols, oxidized derivatives of cholesterol, as inhibitors of HBV infection. Thus, the HepG2-hNTCP-C4 cell line established in this study is a useful tool for the identification of inhibitors of HBV infection as well as for the analysis of the molecular mechanisms of HBV infection.

1. Introduction

Approximately 350 million people are estimated to be infected with hepatitis B virus (HBV) worldwide [1–4]. Chronically infected patients are at a greater risk of developing hepatocellular carcinoma. Currently, clinical treatment for HBV infection includes interferon (IFN)α and nucleos(t)ide analogs [2,4]. IFNα therapy yields long-term clinical benefit in less than 40% of the treated patients and can cause significant side effects. Nucleos(t)ide analog treatment can suppress HBV replication with substantial biochemical and histological improvement; however, such analogs may select drug-resistant viruses, thereby limiting the efficacy of long-term treatment. Thus, the development of new anti-HBV agents targeting a different molecule in the HBV life cycle is urgently needed.

HBV is a hepatotropic virus that mainly or exclusively infects human liver [1,5]. HBV infection can be reproduced in cell culture using primary human hepatocytes (PHH), primary tupaia hepatocytes (PTH), and HepaRG cells [6]. Although HBV infection into these cells is robust, these models have significant limitations as tools for analyzing the mechanisms of HBV infection. Notably, these models can yield unstable reproducibility among lots and low tolerability of transfection efficiency with plasmid and siRNA: preparation and culturing of these cells require significant

Abbreviations: Ab, antibody; cccDNA, covalently closed circular DNA; Cs, cyclosporin; DMSO, dimethyl sulfoxide; GEq, genome equivalent; HBc, HBV core protein; HBs, HBV surface protein; HBV, hepatitis B virus; NTCP, sodium taurocholate cotransporting polypeptide; OHC, hydroxycholesterol; PHH, primary human hepatocytes; PTH, primary tupaia hepatocytes.

* Corresponding author at: Department of Virology II, National Institute of Infectious Diseases, 1-23-1 Toyama, Shinjuku-ku, Tokyo 162-8640, Japan. Fax: +81 3 5285 1161.
E-mail address: kwatashi@nih.go.jp (K. Watashi).

0006-291X/$ - see front matter © 2013 The Authors. Published by Elsevier Inc. All rights reserved.
http://dx.doi.org/10.1016/j.bbrc.2013.12.052

technical skill. In the case of hepatitis C virus (HCV), development of the HCV cell culture (HCVcc) system, in which HCV produced from a JFH-1 strain-based molecular clone can reinfect Huh-7 cells, greatly contribute to the characterization of the HCV life cycle and the evaluation of novel anti-HCV drug candidates [7]. However, the above-noted limitations of HBV-susceptible cells have hampered analysis of the HBV life cycle and impeded identification of new anti-HBV drug targets. Thus, establishment of a novel cell line supporting HBV infection is expected to accelerate the molecular analyses of HBV infection as well as the development of anti-HBV agents.

Recently, the sodium taurocholate cotransporting polypeptide (NTCP) membrane transporter was reported as an HBV entry receptor [8]. NTCP is a sodium-dependent transporter for taurocholic acid, and belongs to a family of solute carrier proteins that consist of seven members (SLC10A1-A7) [9,10]. NTCP is expressed at the basolateral membrane of hepatocytes and mediates the transport of conjugated bile acids and some drugs from portal blood to the liver [11]. NTCP specifically interacts with the large surface protein of HBV, thereby functioning as a viral entry receptor [8].

In this study, we established a strain of HepG2 cells engineered to overexpress the NTCP-encoding gene. One of these clones, designated HepG2-hNTCP-C4, was shown to be highly susceptible for HBV infection, confirming that this infection is mediated by NTCP and permitting evaluation in these cells of the anti-HBV activity of various compounds: reduction of HBV infection of HepG2-hNTCP-C4 cells was observed upon treatment with compounds that blocked HBV entry in other assays and by known inhibitors of NTCP transporter activity [12]. A small-scale chemical screen permitted use to identify oxysterols as inhibitors of HBV infection. Thus, the cell line established in this study is useful for screening for anti-HBV agents, as well as for analysis of the molecular mechanisms of HBV infection.

2. Materials and methods

2.1. Reagents

Dimethyl sulfoxide (DMSO), anti-FLAG antibody (Ab), dextran sulfate, cholate, progesterone, 22(S)-hydroxycholesterol (OHC), 25-OHC, 20α-OHC, and 7β-OHC were purchased from Sigma. Ursodeoxycholate was purchased from Tokyo Chemical Industry. Bromosulfophthalein was from MP biomedicals. Cyclosporin (Cs)A, CsB, CsC, CsD, and CsH were obtained from Enzo Lifesciences. Anti-HBV surface protein (HBs) Ab was from Abcam. Heparin was obtained from Mochida Pharmaceuticals. Myrcludex-B was kindly provided by Dr. Stephan Urban at University Hospital Heidelberg and was synthesized by CS Bio (Shanghai, China).

2.2. Cell culture and plasmid transfection

HepG2 and HepG2-hNTCP-C4 cells were cultured with DMEM/F-12 + GlutaMax (Invitrogen) supplemented with 10 mM HEPES (Invitrogen), 200 units/ml penicillin, 200 μg/ml streptomycin, 10% FBS, 50 μM hydrocortisone and 5 μg/ml insulin in the presence (HepG2-hNTCP-C4 cells) or absence (HepG2 cells) of 400 μg/ml G418 (Nacalai). HepAD38 (kindly provided by Dr. Christoph Seeger at Fox Chase Cancer Center) [13] and HepaRG cells (BIOPREDIC) were cultured as described previously [14].

An expression plasmid for hNTCP [15] was transfected into HepG2 cells with TransIT-LT1 (Mirus) according to the manufacturer's instruction to establish HepG2-hNTCP-C4 cells.

2.3. HBV preparation and infection

HBV was prepared and infected as described [14]. Except as noted, the HBV used in this study was genotype D derived from HepAD38 cells [13]. HBV was infected into NTCP-expressing HepG2 cells at 6×10^3 or 1.8×10^4 genome equivalent (GEq)/cell or into HepaRG cells at 6×10^3 GEq/cell. All infections were performed in the presence of 4% PEG8000 at 37 °C for 16 h as previously described [14]. Dr. Urban's group reported that a quantity of more than 10^4 GEq/cell (i.e. $1.25 - 40 \times 10^4$ GEq/cell) of HBV derived from HepAD38 or HepG2.2.15 cells was required as an inoculum for efficient infection into HepaRG cells in the presence of 4% PEG8000 [16]. A limited number of infections were performed with HBV of genotype C, derived from the serum of an HBV-infected patient, at 100 GEq/cell.

2.4. Real-time PCR and RT-PCR

Real-time PCR for quantification of HBV covalently closed circular (ccc)DNA were performed as described [14]. Isolation of total RNA from cell lysates and reverse transcription PCR (RT-PCR) using a One step RNA PCR kit (Takara) were performed as described previously [17]. Primers used in this study were as follows: 5′-AGGGAGGAGGTGGCAATCAAGAGTGG-3′ and 5′-CCGGCTGAAGAACATTGAGGCACTGG-3′ for NTCP, 5′-CCATGGAGAAGGCTGGGG-3′ and 5′-CAAAGTTGTCATGGATGACC-3′ for GAPDH, respectively.

2.5. Detection of HBs and HBe antigens

HBs antigen was quantified by ELISA as described previously [14]. HBe antigen was detected by Chemiluminescent Immuno Assay (Mitsubishi Chemical Medience).

2.6. Southern blot analysis

Isolation of cellular DNA and southern blot analysis to detect HBV DNAs were performed as described previously [14].

2.7. Indirect immunofluorescence analysis

Immunofluorescence was conducted essentially as described [14] using an anti-HBc Ab (#B0586, DAKO) at a dilution of 1:1000.

2.8. Flow cytometry

An aliquot of 1×10^6 of HepG2 or HepG2-hNTCP-C4 cells was incubated for 30 min with a 1:50 dilution of anti-NTCP Ab (Abcam), then washed and incubated with a dye-labeled secondary Ab (Alexa Fluor 488, Invitrogen) at 1:500 dilution in the dark. Staining and washing were carried out at 4 °C in PBS supplemented with 0.5% bovine serum albumin and 0.1% sodium azide. The signals were analyzed with Cell Sorter SH8000 (SONY).

2.9. siRNA transfection

siRNAs were transfected into the cells at a final concentration of 10–30 nM using Lipofectamine RNAiMAX (Invitrogen) according to the manufacturer's protocol. siRNAs were purchased from Sigma.

2.10. Statistical analyses

Statistical analyses are done with student *t*-test.

3. Results and discussion

3.1. Establishment of a cell line susceptible to HBV infection

To establish a cell line permanently expressing NTCP, we transfected an NTCP-encoding plasmid into HepG2 cells and selected with G418 at 1 mg/ml for 3 weeks. The resultant 9 cell clones were isolated and NTCP expression was analyzed by RT-PCR. One of these clones, designated HepG2-hNTCP-C4, was used in the following experiments because this specific clone exhibited high expression of NTCP and high susceptibility to HBV infection, as shown below. Specifically, NTCP mRNA was abundantly expressed in HepG2-hNTCP-C4 cells, in contrast to little to no expression of NTCP mRNA in the parental HepG2 cells (Fig. 1A). Consistent with the mRNA levels, NTCP protein was detected on the cell surface in HepG2-hNTCP-C4 cells (Fig. 1B). To evaluate HBV infection, these cells were inoculated with HBV for 16 h and cultured in normal growth medium for an additional 12 days, and then HBV surface protein (HBs) and HBe antigens in the culture supernatant as well as HBV DNAs, covalently closed circular (ccc)DNA, and HBV core (HBc) in the cells were assessed. The HBV inoculum used in this experiment was of genotype D, and was derived from the culture supernatant of HepAD38 cells that produce HBV by depletion of tetracycline [13]. To confirm that the detected signals were derived from HBV infection and did not represent non-specific background, the cells were incubated with 1 μM Myrcludex-B (or with DMSO vehicle) for 3 h prior to and for 16 h during HBV infection. Myrcludex-B is a lipopeptide consisting of amino acid residues 2–48 of the pre-S1 region of HBV, and is known to block HBV entry [18]. Following HBV exposure, little or no HBs and HBe antigens was detected in the culture supernatant of the parental HepG2 cells, and little HBc protein was observed in these cells (Fig. 1C, D, and G). However, these proteins, as well as HBV DNAs and cccDNA, were detected in HBV-treated HepG2-hNTCP-C4 cells (Fig. 1C–G). The corresponding signals were significantly reduced in the cells treated with an HBV entry inhibitor, Myrcludex-B, but not in the cells treated with DMSO (Fig. 1C–G). These data suggested that HepG2-hNTCP-C4 cells are HBV-susceptible, in contrast to the parental HepG2 cells. The HepG2-hNTCP-C4 cell line also was susceptible to infection with HBV genotype C, which was derived from the serum of an HBV-infected patient (Fig. 1H and I).

3.2. HBV susceptibility of HepG2-hNTCP-C4 cells was augmented by pretreatment with DMSO

It has been reported that a prolonged HBV infection in primary human hepatocytes can be enhanced by pretreatment with DMSO [19]. Therefore, we examined whether pretreatment with DMSO affected HBV infection of HepG2-NTCP-C4 cells. The cells were pretreated with 3% DMSO for 24 h and then the HBV infectivity was investigated following the protocol as in Fig. 1. Immunofluorescence analysis revealed that approximately 50% of the DMSO-pretreated cells were HBc-positive at 12 days post-infection (Fig. 2A, middle), while only 10–20% of cells were HBc-positive cells in the absence of pretreatment (Fig. 1G, upper right). The effect of DMSO pretreatment on HBV susceptibility was both concentration-(Fig. 2B) and time-dependent (Fig. 2C).

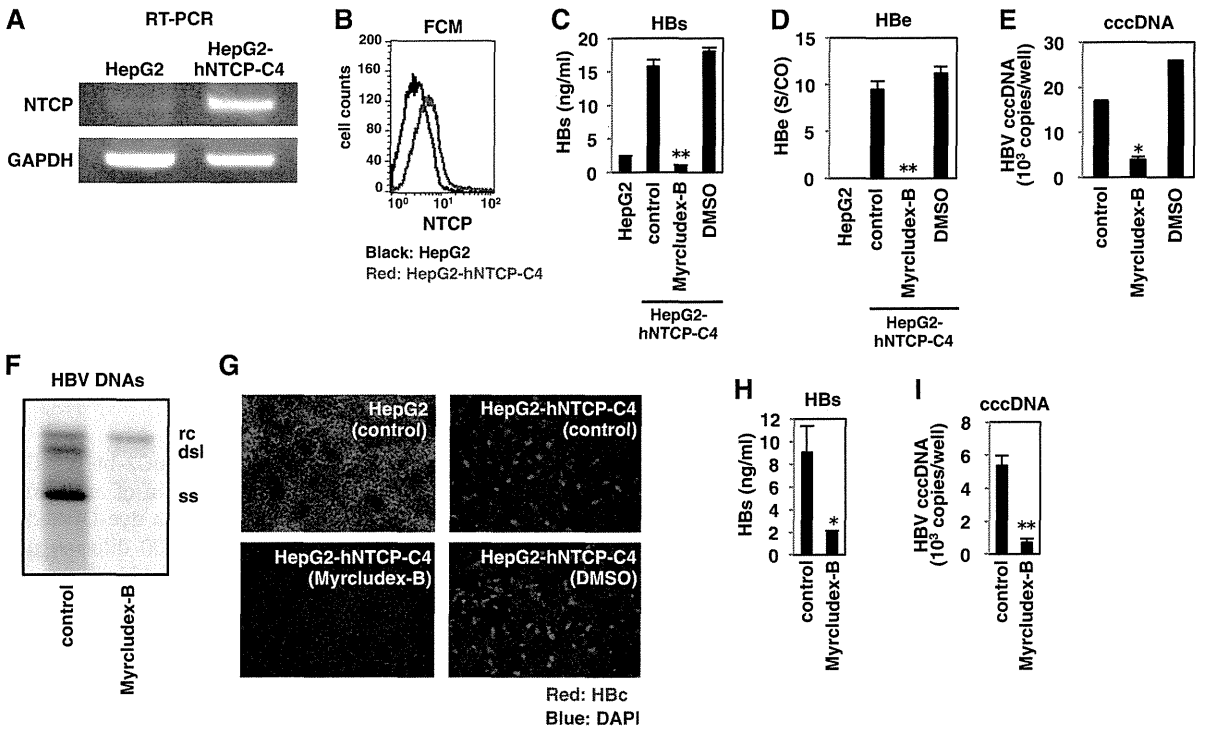

Fig. 1. Establishment of a cell line susceptible to hepatitis B virus (HBV) infection. (A) mRNAs for sodium taurocholate cotransporting polypeptide (NTCP) and GAPDH in HepG2 and HepG2-hNTCP-C4 cells were detected by RT-PCR. (B) NTCP protein on cell surface of HepG2 (black) and HepG2-hNTCP-C4 cells (red) was detected by flow cytometry. (C-G) HepG2-hNTCP-C4 or the parental HepG2 cells pretreated with or without 1 μM Myrcludex-B or vehicle (DMSO) for 3 h were inoculated with HBV (genotype D) for 16 h. After washing out of the free virus and the compounds, the cells were cultured for an additional 12 days in normal growth medium and then assayed for secretion of HBs (C) and HBe antigens (D) secreted in the culture supernatant, and for the presence of HBV covalently closed circular (ccc)DNA (E), HBV DNAs (F), and HBV core (HBc) proteins (G) in the cells. rc, dsl, and ss in (F) indicate relaxed circular, double strand linear, and single strand HBV DNA, respectively. Red and blue signals in (G) indicate HBc protein and nuclear staining, respectively. (H and I) Infection of blood-borne HBV into HepG2-hNTCP-C4 cells. HBV (genotype C) derived from an HBV-infected patient was used as an inoculum for the infection assay. Levels for HBs antigen in the culture supernatant (H) and HBV cccDNA in the cells (I) are shown. The data in C–E, H, and I show the means of three independent experiments. $^{*}P < 0.05$, $^{**}P < 0.01$.

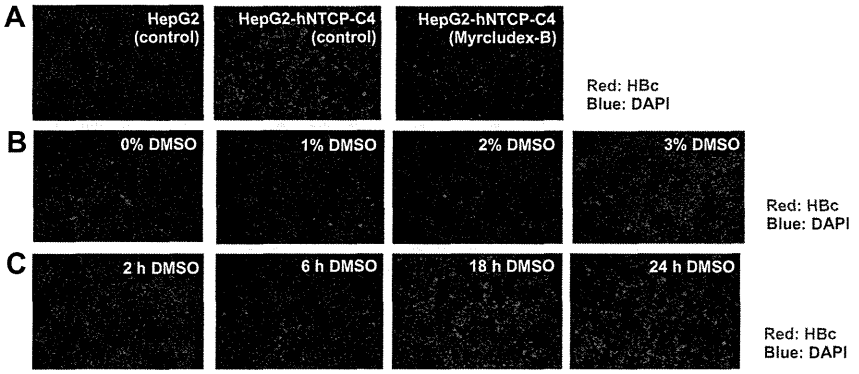

Fig. 2. HBV infection was facilitated by pretreatment of HepG2-hNTCP-C4 cells with DMSO. (A) HepG2 or HepG2-hNTCP-C4 cells preincubated with 3% DMSO for 24 h were inoculated with HBV in the presence of 3% DMSO for 16 h. Treatment with Myrcludex-B was used as a negative control for infection. At 12 days postinfection, HBc protein (red) and the nucleus (blue) were detected by immunofluorescence analysis. (B) Cells were pretreated by exposure for 24 h to various concentrations of DMSO (0–3%). (C) Cells were pretreated by exposure to 3% DMSO for various treatment times (2, 6, 18, and 24 h). HBc protein (red) and the nucleus (blue) were detected as in (A).

3.3. HBV infection was mediated by NTCP in HepG2-hNTCP-C4 cells

We used knockdown analysis to determine whether HBV infection of HepG2-hNTCP-C4 cells was mediated by NTCP. Transfection with siRNA against NTCP (si-NTCP) and GAPDH (si-GAPDH) specifically knocked down mRNA for NTCP and GAPDH, respectively, in HepG2-hNTCP-C4 cells (Fig. 3A). Consistent with the effect on transcript level, treatment with si-NTCP depleted NTCP protein on the cell surface (Fig. 3B). The HBV infection assay, performed as in Fig. 1, indicated that depletion of NTCP reduced the levels for HBs (Fig. 3C) and HBe antigens (Fig. 3D) in culture supernatant as well as HBV cccDNA (Fig. 3E) and HBc protein (Fig. 3F) in the cells at 12 days postinfection with HBV. These data suggested that HBV infection into HepG2-hNTCP-C4 cells was mediated by NTCP.

3.4. Evaluation of HBV entry inhibitors in HepG2-hNTCP-C4 cells

To determine whether HepG2-hNTCP-C4 cells could be used to evaluate anti-HBV activity of compounds, we examined the effect of known entry inhibitors in these cells. The cells were pretreated with compounds for 3 h and then inoculated with HBV for 16 h in the presence of compounds (Fig. 4A). Inoculation with HBV was followed by culturing of the cells in normal growth medium for an additional 12 days until detection of HBs antigen in the culture supernatant and cccDNA in the cells (Fig. 4A). This protocol has been used previously to evaluate the entry inhibition activity of compounds [20]. Treatment with anti-HBs neutralizing Ab, but not that with a non-relevant anti-FLAG Ab, inhibited HBV infection (Fig. 4B). Heparin and dextran sulfate, which have been reported to inhibit HBV attachment to the target cells [21], also reduced HBV infection (Fig. 4C). In addition, known NTCP substrates and inhibitors, including ursodeoxycholate, cholate, progesterone, and bromosulfophthalein [12], blocked HBV infection in this assay (Fig. 4D). We recently identified that cyclosporin A (CsA) and its analogs blocked HBV entry through inhibition of interaction between NTCP and the HBV large surface protein [20]. As shown in Fig. 4E, CsA and its analogs inhibited HBV infection in the present assay, with CsB showing the highest potency for inhibition of HBV infection among Cs analogs (Fig. 4E). These data indicate that HepG2-hNTCP-C4 cells are useful for evaluating the effect of HBV entry inhibitors.

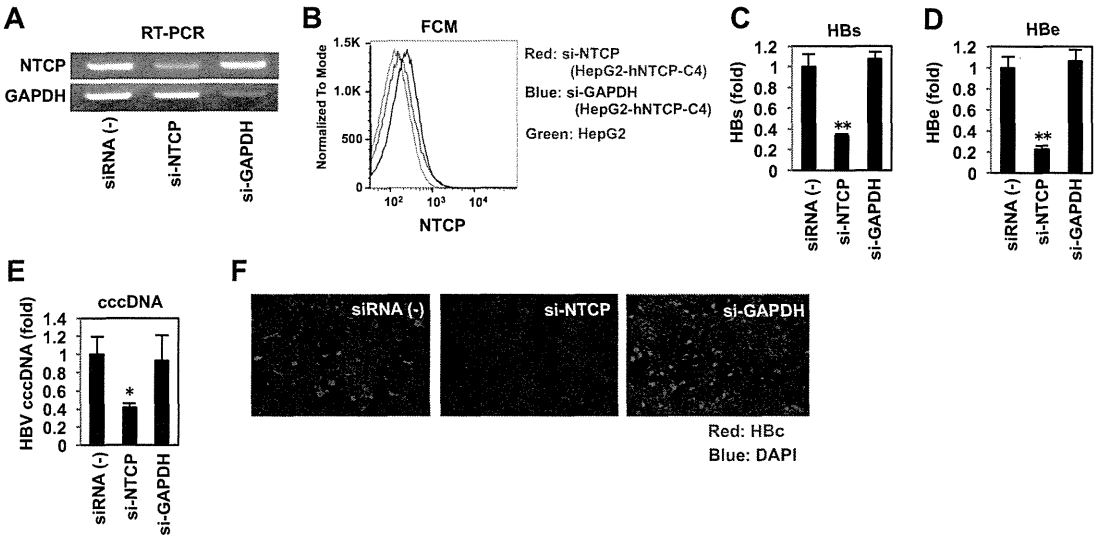

Fig. 3. HBV infection of HepG2-hNTCP-C4 cells was mediated by NTCP. (A) HepG2-hNTCP-C4 cells were transfected (for 48 h) with or without [siRNA(−)] siRNAs against NTCP (si-NTCP) or GAPDH (si-GAPDH), and mRNA expression levels of NTCP and GAPDH were detected by RT-PCR. (B) Parental HepG2 and HepG2-hNTCP-C4 cells were transfected (for 48 h) with or without si-NTCP or si-GAPDH, and cell surface-displayed NTCP protein was detected by flow cytometry. The red, blue, and green lines indicate the signal in HepG2-hNTCP-C4 cells treated with si-NTCP, HepG2-hNTCP-C4 cells treated with si-GAPDH, and HepG2 cells, respectively. (C–F) The cells prepared as in (A) were infected with HBV according to the protocol shown in Fig. 1. Culture supernatants were assayed for levels of secreted HBs (C) and HBe (D) antigens, and cells were assayed for intracellular levels of HBV cccDNA (E) and HBc protein (F). The red and blue signals in (F) indicate HBc and nuclear staining, respectively.

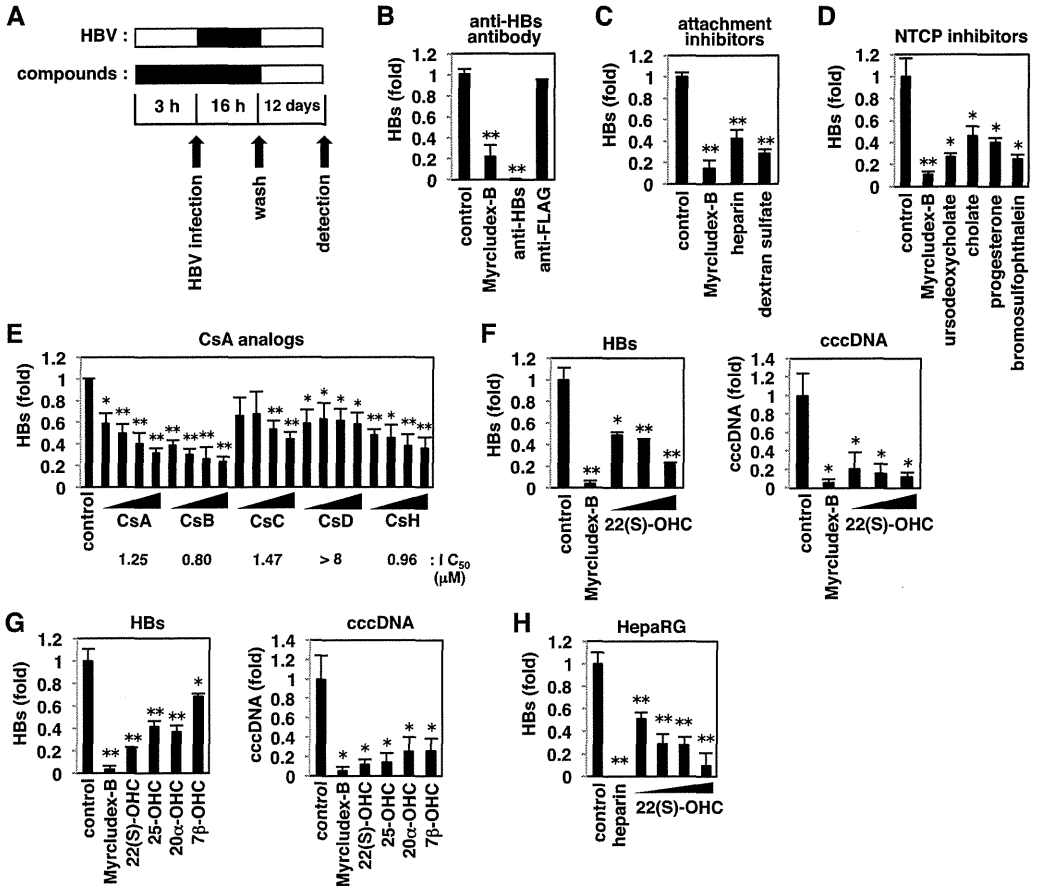

Fig. 4. Evaluation of HBV entry inhibitors in HepG2-hNTCP-C4 cells. (A) Schematic representation of the experimental procedure for evaluating HBV entry inhibition. HepG2-hNTCP-C4 cells were pretreated with or without compounds for 3 h and then inoculated with HBV for 16 h. After washing out of free HBV and the compounds, the cells were cultured with normal culture medium in the absence of compounds for an additional 12 days, and HBs antigen in the culture supernatant and/or HBV cccDNA in the cells were detected. Black and white bars show period of treatment and without treatment, respectively. (B–G) HepG2-hNTCP-C4 cells were treated with or without 1 μM Myrcludex-B, 10 μg/ml anti-HBs or anti-FLAG Ab (B); HBV attachment inhibitors including 100 IU/ml heparin and 1 mg/ml dextran sulfate (C); NTCP inhibitors including 100 μM ursodeoxycholate, 100 μM cholate, 40 μM progesterone, and 100 μM bromosulfophthalein (D); cyclosporins (CsA, CsB, CsC, CsD, CsH) at 1, 2, 4, and 8 μM (E); 22(S)-hydroxycholesterol (OHC) at 11, 33, and 100 μM (F); or oxysterols including 22(S)-OHC, 25-OHC, 20α-OHC, and 7β-OHC at 100 μM (G). For each assay, the cells were infected with HBV as shown in (A) and the levels of HBs antigen secreted into the culture supernatant and/or cccDNA in the cells were detected. Pretreatment time of compounds in (F) and (G) was 6 h, instead of 3 h. IC_{50}s of cyclosporin derivatives calculated in this assay are shown below the graph in (E). (H) HepaRG cells were treated with or without various concentrations of 22(S)-OHC (0.3, 0.9, 3, and 9 μM) and infected with HBV according to the protocol shown in (A). HBV infection was monitored by detecting the level of HBs secreted into the culture supernatant.

As there are only reverse transcriptase inhibitors currently available as anti-HBV drugs that inhibit the HBV life cycle, development of new anti-HBV agents targeting different steps in the HBV life cycle are greatly needed [1–4]. We therefore screened for compounds that blocked HBV entry by following the same protocol as in Fig. 4A. We found that an oxysterol, 22(S)-hydroxycholesterol (OHC), reduced HBV infection in a dose-dependent manner (Fig. 4F). Other oxysterols, 25-OHC, 20α-OHC, and 7β-OHC, also significantly decreased HBV infection (Fig. 4G). To validate this result, we repeated the assay using HepaRG cells, a line that frequently has been used in HBV entry experiments [14]. We found that 22(S)-OHC also reduced HBV infection of HepaRG cells in a dose-dependent manner (Fig. 4H), suggesting that the observed inhibitory effect of oxysterols reflects a genuine inhibition of HBV infection.

Thus, we have newly established a cell line that is susceptible to HBV infection. HepG2-hNTCP-C4 cells exhibited approximately 50% of HBV-infection positive cells (Fig. 2A), while maximum HBV infection of HepaRG cells was reported to be only 7% [16] or 20% [22] of the total population. These cells are expected to be useful for analyzing the molecular mechanisms of HBV infection, given that HepG2-derived cells show higher efficiency of transfection with expression plasmids and siRNAs than the current available HBV-susceptible PHH, PTH, and HepaRG cells. HepG2-hNTCP-C4 cells will facilitate knockdown analysis of host factors to define their roles in infection and screenings of compounds to identify novel inhibitors of HBV infection. As an example, we demonstrated here that oxysterols blocked HBV infection. The molecular mechanisms whereby oxysterols inhibit HBV infection are now under investigation. These analyses will be important for understanding the mechanisms of HBV infection as well as for developing new anti-HBV agents.

Acknowledgments

HepAD38 cells were kindly provided by Dr. Christoph Seeger at Fox Chase Cancer Center. Myrcludex-B, a pre-S1 lipopeptide, was kindly provided by Dr. Stephan Urban at University Hospital Heidelberg. We also are grateful to all of the members of Department of Virology II, National Institute of Infectious Diseases. This study was supported by Grants-in-aid from the Ministry of Health, Labor, and Welfare, Japan, from the Ministry of Education, Culture, Sports, Science, and Technology, Japan, and from Japan Society for the Promotion of Science, and from the Research on Health Sciences Focusing on Drug Innovation from the Japan Health Sciences Foundation.

References

[1] D. Grimm, R. Thimme, H.E. Blum, HBV life cycle and novel drug targets, Hepatol. Int. 5 (2011) 644–653.

[2] J.M. Pawlotsky, G. Dusheiko, A. Hatzakis, D. Lau, G. Lau, T.J. Liang, S. Locarnini, P. Martin, D.D. Richman, F. Zoulim, Virologic monitoring of hepatitis B virus therapy in clinical trials and practice: recommendations for a standardized approach, Gastroenterology 134 (2008) 405–415.

[3] M. Rapicetta, C. Ferrari, M. Levrero, Viral determinants and host immune responses in the pathogenesis of HBV infection, J. Med. Virol. 67 (2002) 454–457.

[4] F. Zoulim, Hepatitis B virus resistance to antiviral drugs: where are we going?, Liver Int 31 (Suppl. 1) (2011) 111–116.

[5] P. Gripon, S. Rumin, S. Urban, J. Le Seyec, D. Glaise, I. Cannie, C. Guyomard, J. Lucas, C. Trepo, C. Guguen-Guillouzo, Infection of a human hepatoma cell line by hepatitis B virus, Proc. Natl. Acad. Sci. USA 99 (2002) 15655–15660.

[6] D. Glebe, S. Urban, Viral and cellular determinants involved in hepadnaviral entry, World J. Gastroenterol. 13 (2007) 22–38.

[7] J.M. Gottwein, J. Bukh, Cutting the gordian knot-development and biological relevance of hepatitis C virus cell culture systems, Adv. Virus Res. 71 (2008) 51–133.

[8] H. Yan, G. Zhong, G. Xu, W. He, Z. Jing, Z. Gao, Y. Huang, Y. Qi, B. Peng, H. Wang, L. Fu, M. Song, P. Chen, W. Gao, B. Ren, Y. Sun, T. Cai, X. Feng, J. Sui, W. Li, Sodium taurocholate cotransporting polypeptide is a functional receptor for human hepatitis B and D virus, Elife 1 (2012) e00049.

[9] M.S. Anwer, B. Stieger, Sodium-dependent bile salt transporters of the SLC10A transporter family: more than solute transporters, Pflugers Arch. (2013) (Epub ahead of print).

[10] P.J. Meier, B. Stieger, Bile salt transporters, Annu. Rev. Physiol. 64 (2002) 635–661.

[11] C. Seeger, W.S. Mason, Sodium-dependent taurocholic cotransporting polypeptide: a candidate receptor for human hepatitis B virus, Gut 62 (2013) 1093–1095.

[12] R.B. Kim, B. Leake, M. Cvetkovic, M.M. Roden, J. Nadeau, A. Walubo, G.R. Wilkinson, Modulation by drugs of human hepatic sodium-dependent bile acid transporter (sodium taurocholate cotransporting polypeptide) activity, J. Pharmacol. Exp. Ther. 291 (1999) 1204–1209.

[13] S.K. Ladner, M.J. Otto, C.S. Barker, K. Zaifert, G.H. Wang, J.T. Guo, C. Seeger, R.W. King, Inducible expression of human hepatitis B virus (HBV) in stably transfected hepatoblastoma cells: a novel system for screening potential inhibitors of HBV replication, Antimicrob. Agents Chemother. 41 (1997) 1715–1720.

[14] K. Watashi, G. Liang, M. Iwamoto, H. Marusawa, N. Uchida, T. Daito, K. Kitamura, M. Muramatsu, H. Ohashi, T. Kiyohara, R. Suzuki, J. Li, S. Tong, Y. Tanaka, K. Murata, H. Aizaki, T. Wakita, Interleukin-1 and tumor necrosis factor-alpha trigger restriction of hepatitis B virus infection via a cytidine deaminase activation-induced cytidine deaminase (AID), J. Biol. Chem. 288 (2013) 31715–31727.

[15] S. Mita, H. Suzuki, H. Akita, H. Hayashi, R. Onuki, A.F. Hofmann, Y. Sugiyama, Inhibition of bile acid transport across Na+/taurocholate cotransporting polypeptide (SLC10A1) and bile salt export pump (ABCB 11)-coexpressing LLC-PK1 cells by cholestasis-inducing drugs, Drug Metab. Dispos. 34 (2006) 1575–1581.

[16] A. Schulze, K. Mills, T.S. Weiss, S. Urban, Hepatocyte polarization is essential for the productive entry of the hepatitis B virus, Hepatology 55 (2012) 373–383.

[17] M. Koyanagi, M. Hijikata, K. Watashi, O. Masui, K. Shimotohno, Centrosomal P4.1-associated protein is a new member of transcriptional coactivators for nuclear factor-kappaB, J. Biol. Chem. 280 (2005) 12430–12437.

[18] P. Gripon, I. Cannie, S. Urban, Efficient inhibition of hepatitis B virus infection by acylated peptides derived from the large viral surface protein, J. Virol. 79 (2005) 1613–1622.

[19] P. Gripon, C. Diot, A. Corlu, C. Guguen-Guillouzo, Regulation by dimethylsulfoxide, insulin, and corticosteroids of hepatitis B virus replication in a transfected human hepatoma cell line, J. Med. Virol. 28 (1989) 193–199.

[20] K. Watashi, A. Sluder, T. Daito, S. Matsunaga, A. Ryo, S. Nagamori, M. Iwamoto, S. Nakajima, S. Tsukuda, K. Borroto-Esoda, M. Sugiyama, Y. Tanaka, Y. Kanai, H. Kusuhara, M. Mizokami, T. Wakita, Cyclosporin A and its analogs inhibit hepatitis B virus entry into cultured hepatocytes through targeting a membrane transporter NTCP, Hepatology, in press.

[21] A. Schulze, P. Gripon, S. Urban, Hepatitis B virus infection initiates with a large surface protein-dependent binding to heparan sulfate proteoglycans, Hepatology 46 (2007) 1759–1768.

[22] O. Hantz, R. Parent, D. Durantel, P. Gripon, C. Guguen-Guillouzo, F. Zoulim, Persistence of the hepatitis B virus covalently closed circular DNA in HepaRG human hepatocyte-like cells, J. Gen. Virol. 90 (2009) 127–135.

FEBS Letters 587 (2013) 2377–2384

FEBS Letters

journal homepage: www.FEBSLetters.org

Selective control of SNARE recycling by Golgi retention

Masayoshi Fukasawa [a], Anda Cornea [b], Oleg Varlamov [c,*]

[a] Department of Biochemistry and Cell Biology, National Institute of Infectious Diseases, Tokyo, Japan
[b] Imaging and Morphology Support Core, Oregon National Primate Research Center, Beaverton, OR 97006, United States
[c] Division of Diabetes, Obesity and Metabolism, Oregon National Primate Research Center, Beaverton, OR 97006, United States

ARTICLE INFO

Article history:
Received 6 March 2013
Revised 4 June 2013
Accepted 4 June 2013
Available online 20 June 2013

Edited by Felix Wieland

Keywords:
Golgi
SNARE
Recycling
Retention
Endoplasmic reticulum
ER
Lipid raft
Membrane fusion
Vesicle
Dynamic equilibrium
i-SNARE
Homotypic fusion
Golgi tether
Entropy

ABSTRACT

Two distinct sets of soluble *N*-ethylmaleimide-sensitive factor attachment protein receptors (SNARE) catalyze membrane fusion in the *cis*-Golgi and *trans*-Golgi. The mechanism that controls Golgi localization of SNAREs remains largely unknown. Here we tested three potential mechanisms, including vesicle recycling between the Golgi and the endoplasmic reticulum, partitioning in Golgi lipid microdomains, and selective intra-Golgi retention. Recycling rates showed a linear relationship with intra-Golgi mobility of SNAREs. The *cis*-Golgi SNAREs had higher mobility than intra-Golgi SNAREs, whereas vesicle SNAREs had higher mobility than target membrane SNAREs. The differences in SNARE mobility were not due to preferential partitioning into detergent-resistant membrane microdomains. We propose that intra-Golgi retention precludes entropy-driven redistribution of SNAREs to the endoplasmic reticulum and endocytic compartments.

1. Introduction

The Golgi apparatus is a polarized organelle that mediates protein transport between the endoplasmic reticulum (ER) and endocytic compartments. The *cis*-Golgi is a receiver of anterograde vesicles traveling from the ER, whereas the *trans*-Golgi is a departure site for vesicles traveling to endocytic compartments [1]. The ER resident proteins that escape to the Golgi and Golgi proteins cycle back to the ER via the retrograde pathway [2–9].

Soluble *N*-ethylmaleimide-sensitive factor attachment protein receptors (SNAREs) [10] play a fundamental role in membrane fusion and have a polarized, gradient-like distribution in the Golgi. The vesicle (*v*)-SNARE proteins rBet1 [11,12], and the target membrane (*t*)-SNAREs Ers24 (Sec22) [12,13], p27 (Gs27, membrin) [14,15] are enriched in the *cis*-Golgi, whereas the *t*-SNAREs Syntaxin5 (Sed5) [16,17], Gos28 (Gs28, p28, Gos1p) [18–20] and Ykt6 [21] and the *v*-SNARE Gs15 (Sft1) [21,22] are enriched intra-Golgi and in the *trans*-Golgi. Morphological and biochemical studies suggest that at least two SNARE complexes (SNAREpins), the *cis*-Golgi *v*-[rBet1]:*t*-[Ers24-p27-Syntaxin5] and the *trans*-Golgi *v*-[Gs15]:*t*-[Ykt6-Gos28-Syntaxin5], catalyze membrane fusion in the Golgi stack [15,23–26].

While the distribution of Golgi SNAREpins is well established, the mechanisms that control their distribution across the Golgi stack are largely unknown. Here we tested three potential mechanisms responsible for SNARE localization in the Golgi: vesicle-mediated recycling between the Golgi and the ER, selective partitioning in the Golgi membrane microdomains, and selective retention in the Golgi. Finally, we propose a new idea how fusogenic and inhibitory SNARE complexes [27] can generate SNARE gradients in the early secretory pathway.

* Corresponding author. Address: L584, Oregon National Primate Research Center, 505 NW 185th Ave. Beaverton, OR 97006, United States.
E-mail address: varlamov@ohsu.edu (O. Varlamov).

0014-5793/$36.00
http://dx.doi.org/10.1016/j.febslet.2013.06.004

2. Results

2.1. SNARE recycling between the Golgi and the ER

Protein recycling between the Golgi and the ER is mediated by anterograde and retrograde transport (Fig. 1C). We computed the rate of anterograde transport (K_{in}) and the rate of retrograde transport (K_{out}) for various SNARE proteins using fluorescence recovery after photobleaching (FRAP) [28]. The Golgi membrane SNARE proteins rBet1, Ers24, p27, Gos28, Syntaxin5 and Gs15 were tagged with the cyan fluorescent protein (CFP) and expressed in NRK cells as previously described [29]. K_{in} values were calculated from single-exponential fits of fluorescence recovery curves after photobleaching the Golgi (Fig. 1A and B and Supplementary videos), whereas K_{out} values were determined based on fluorescence recovery after photobleaching the ER (Fig. 3 and Supplementary videos).

For all SNARE proteins examined, K_{in} were not significantly different than the corresponding K_{out} values (Fig. 1D and 3B). K_{in} values for rBet1 were significantly higher than K_{in} values for all other SNARE proteins, but no statistically significant differences in K_{in} values were detected between any other combinations of SNAREs (Fig. 1D). To confirm that fluorescence recovery represents the vesicle-mediated transport step that originates in the ER, we treated digitonin-permeabilized cells with the dominant-negative mutant of GTPase Sar1T39N, the inhibitor of COPII vesicle formation at the ER exit sites [30,31]. To verify that fluorescence recovery in

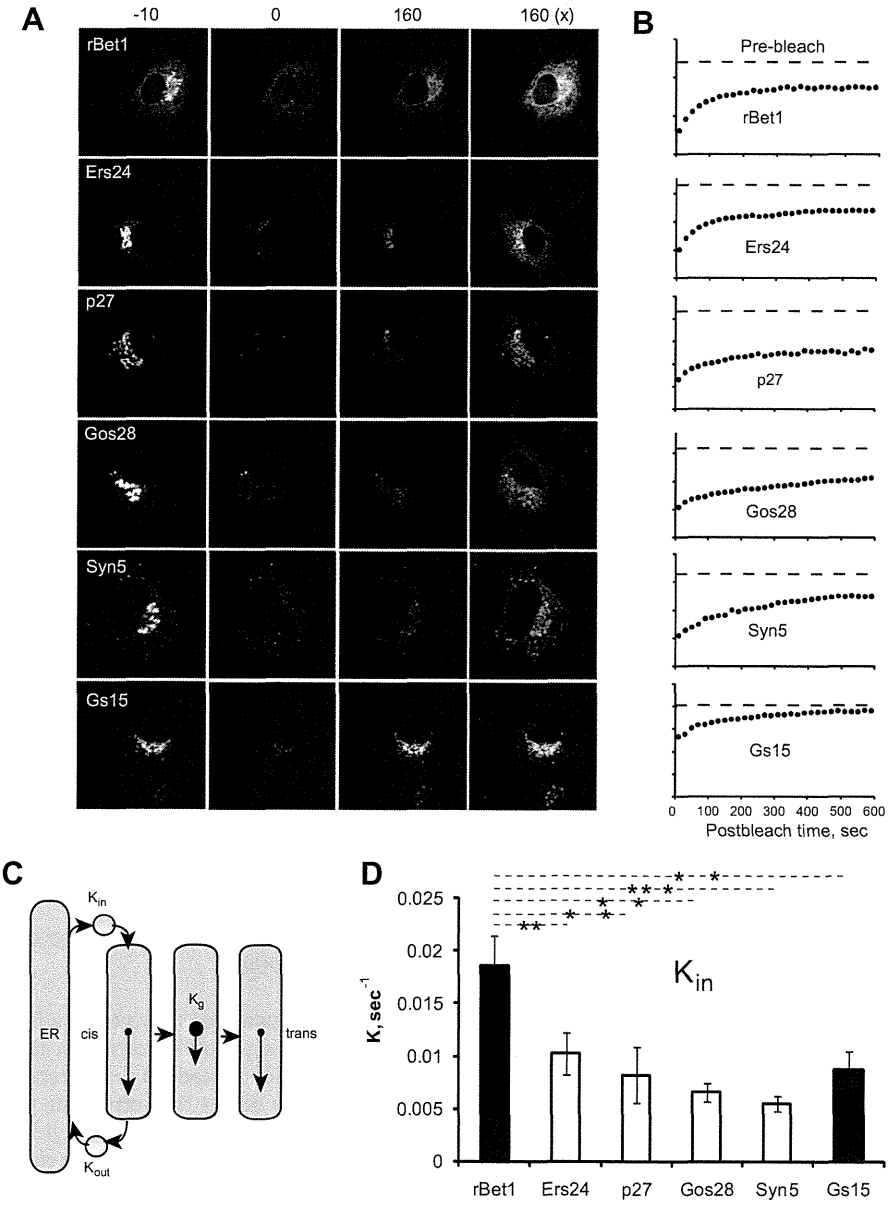

Fig. 1. Anterograde transport of SNARE proteins in the early secretory pathway. CFP-tagged Golgi SNARE proteins were transiently expressed in NRK cells, the Golgi regions were bleached, and anterograde transport rates were determined following fluorescence recovery in the Golgi. (A) Representative images showing the pre-bleaching (−10 s), the post-bleaching (0 s), and the post-recovery stages (160 s) of FRAP. The later set of images is shown at higher contrast (160×). Scale bar = 10 μm. (B) Representative fluorescence traces showing the kinetics of fluorescence recovery in the Golgi following photobleaching. The ordinate represents the arbitrary fluorescence units. (C) Protein recycling in the early secretory pathway. The ER and the Golgi are bound bi-directionally by anterograde transport (represented by the rate K_{in}) and by retrograde transport (represented by the rate K_{out}). Intra-Golgi rates (K_g) represent protein mobility in the Golgi membranes. (D) the Golgi. K_{in} values were calculated from single-exponential fits of fluorescence recovery curves after photobleaching the Golgi as described in Section 5. Bars are means ± S.E.M. for n = 10–15 cells. Statistically significant differences between K_{in} values were determined using One-way ANOVA; $^{**}P < 0.01$; $^{***}P < 0.001$.

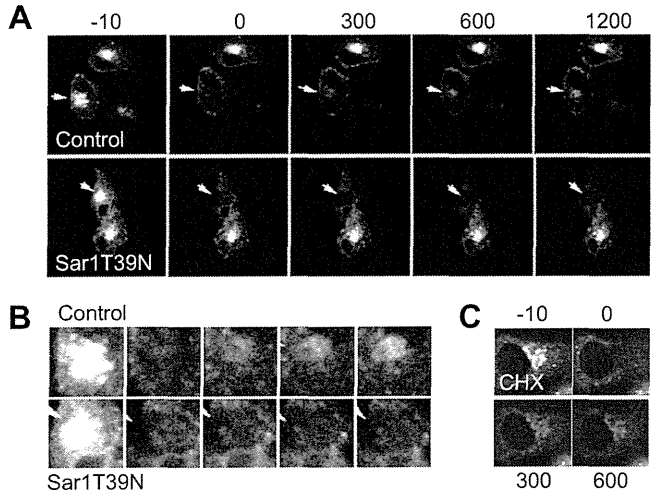

Fig. 2. Anterograde transport of SNAREs requires the ER exit sites. (A) Digitonin-permeabilized cells expressing CFP-GOS28 were incubated with transport mixture in the presence or absence of the dominant-negative mutant Sar1 T39 N. The Golgi regions of permeabilized cells (arrows) were photobleached, and the recovery of fluorescence in the Golgi was monitored as described above. (B) Enlarged image of the Golgi regions from "A". (C) Cells expressing CFP-GOS28 were pretreated for 2 h with 100 μg/ml cycloheximide and the recovery of fluorescence in the Golgi was monitored as described in Section 5.

the Golgi requires membrane fusion, we pretreated intact cells with the membrane fusion inhibitor *N*-ethylmaleimide. Anterograde transport was inhibited by *N*-ethylmaleimide (data not shown), and by Sar1T39N (Fig. 2A and B). Pretreatment of cells with the protein synthesis inhibitor cycloheximide did not alter anterograde transport (Fig. 2C).

K_{out} values for rBet1 were significantly higher than K_{out} values for Gos28, Syntaxin5 and Gs15, although no significant differences between K_{out} for rBet1 and K_{out} for Ers24 and p27 were detected (Fig. 3B). There was a strong linear correlation ($R^2 = 0.96$) between K_{in} and K_{out} values, consistent with the "*trans* < *cis*" distribution of Golgi SNARE proteins [15,23–26]: Syntaxin5 < Gos28 < p27 < Ers24 < rBet1 (Fig. 3C). Thus, the *cis*-Golgi SNAREs cycle at higher rates than intra-Golgi SNAREs. Gs15 was excluded from a linear regression analysis because its K_{in} was higher than what can be expected for the *trans*-Golgi SNARE (Fig. 3C).

2.2. Partitioning of SNARE proteins in membrane microdomains

Recent studies suggest that exocytic SNAREs are enriched in detergent-resistant lipid microdomains (lipid rafts) [32–36]. We thus tested whether Golgi SNARE proteins can also differentially partition into lipid microdomains in NRK and HELA cells. Cells were extracted with the cold non-ionic detergent Lubrol WX followed by sucrose density centrifugation (Supplementary Fig. 1S). Light fractions 3–5 on the sucrose density gradient represent detergent-resistant lipid domains, whereas the bottom fractions represent detergent-soluble lipid domains. Immunoblot analysis of gradient fractions revealed differential partitioning of endogenous secretory pathway proteins into detergent-resistant fractions (Fig. 4). Proteins that were highly enriched in detergent-resistant membranes included Caveolin-1 (plasma membrane, endosomes and TGN), SNAREs Vti1a, Vti1b and Syntaxin6 (endosomes and TGN), Rab6a (GTPase involved in *post*-Golgi and intra-Golgi transport), and TGN38 [37–39]. *Trans*-Golgi SNAREs Gs15, Syntaxin5 and Gos28, and Rab1b (GTPase involved in ER-Golgi and intra-Golgi transport [39]) showed minor partitioning and *cis*-Golgi SNAREs p27, Ers24 and rBet1 were not detected in the detergent-resistant fractions (Fig. 4A and B). When cells were extracted with Triton X-100, none of the proteins examined partitioned into caveolin-containing detergent-resistant fractions (Supplementary Fig. 2S).

Whereas most Golgi SNAREs are integral membrane proteins, Ykt6 is associated with the Golgi membranes via a dual farnesyl/palmitoyl lipid group [40]. Membrane binding of Ykt6 is under the negative intra-molecular regulation of its N-terminal domain that keeps the Ykt6 protein in cytosol [41]. To test whether Ykt6 is associated with detergent-resistant domains, we stably expressed GFP-(wild type Ykt6) and GFP-(F42EYkt6), the open conformation mutant [40], and subjected the cells to Lubrol WX solubilization. The wild type form of GFP-Ykt6 remained cytoplasmic and distributed to the detergent-soluble fraction, whereas GFP-(F42EYkt6) was membrane-bound and partitioned in detergent-resistant lipid fractions (Fig. 4C). We conclude that transmembrane Golgi SNARE proteins are primarily excluded from Lubrol-resistant lipid rafts.

2.3. Intra-Golgi mobility of SNARE proteins

Active retention through protein–protein or protein–lipid interactions may restrict SNARE mobility in the Golgi. To test intra-Golgi mobility of SNARE proteins, we photobleached small areas of the Golgi and followed the recovery of fluorescence as described [42] (Fig. 5A and Supplementary videos). Golgi SNAREs displayed differential mobility. The *cis*-Golgi *v*-SNARE rBet1 and the *trans*-Golgi *v*-SNARE Gs15 had the highest mobility and intra-Golgi *t*-SNAREs Syntaxin5 and Gos28 had the lowest mobility in the Golgi. The recovery of fluorescence after photobleaching Golgi regions for Syntaxin5 and Gos28 was very slow compared to other SNAREs (Fig. 5), suggesting that intra-Golgi SNAREs are largely immobile in the Golgi membranes. This result was reproduced in CHO cells (data not shown).

The *cis*-Golgi SNARE Ers24 was more mobile than the intra-Golgi SNARE Syntaxin5 and the *trans*-Golgi *v*-SNARE Gs15 was more mobile than the *trans*-Golgi *t*-SNAREs Syntaxin5 and Gos28 (Fig. 5B). This analysis suggests that *v*-SNAREs more mobile in the Golgi membranes than *t*-SNAREs.

Further analysis showed the linear relationship between intra-Golgi mobility rates and the rates of anterograde transport of SNARE proteins, consistent with the intra-Golgi distribution of SNAREs: Syntaxin5 < Gos28 < p27 < Ers24 < rBet1 (Fig. 5C). Similarly, intra-Golgi mobility rates correlated with the rates of retrograde transport of SNARE proteins (Fig. 5D). Thus, a selective Golgi retention mechanism may control intra-Golgi localization of SNARE proteins.

3. Discussion

3.1. SNARE recycling between the Golgi and the ER and fractional distillation hypothesis

The Golgi apparatus may utilize a fractional distillation principle for mediating protein sorting in the early secretory pathway [43]. This prediction leads to a new paradigm that the rate at which a Golgi protein enters the retrograde pathway and/or the rate at which an ER protein enters the Golgi may determine the relative partitioning of this protein into the *cis*- and *trans*-Golgi compartments. If this mechanism is true, then the *cis* < *trans* Golgi SNARE gradient is a result of a slower exit from and/or a faster return to the Golgi, while the *cis* > *trans* Golgi SNARE gradient is a result of a faster exit from and/or a slow return to the Golgi.

The present report, however, suggests that for all SNARE proteins examined, anterograde rates (K_{in}) were not significantly different than the corresponding retrograde rates (K_{out}) of transport (Fig. 1D, 3B and C). Thus, it is unlikely that the asymmetric

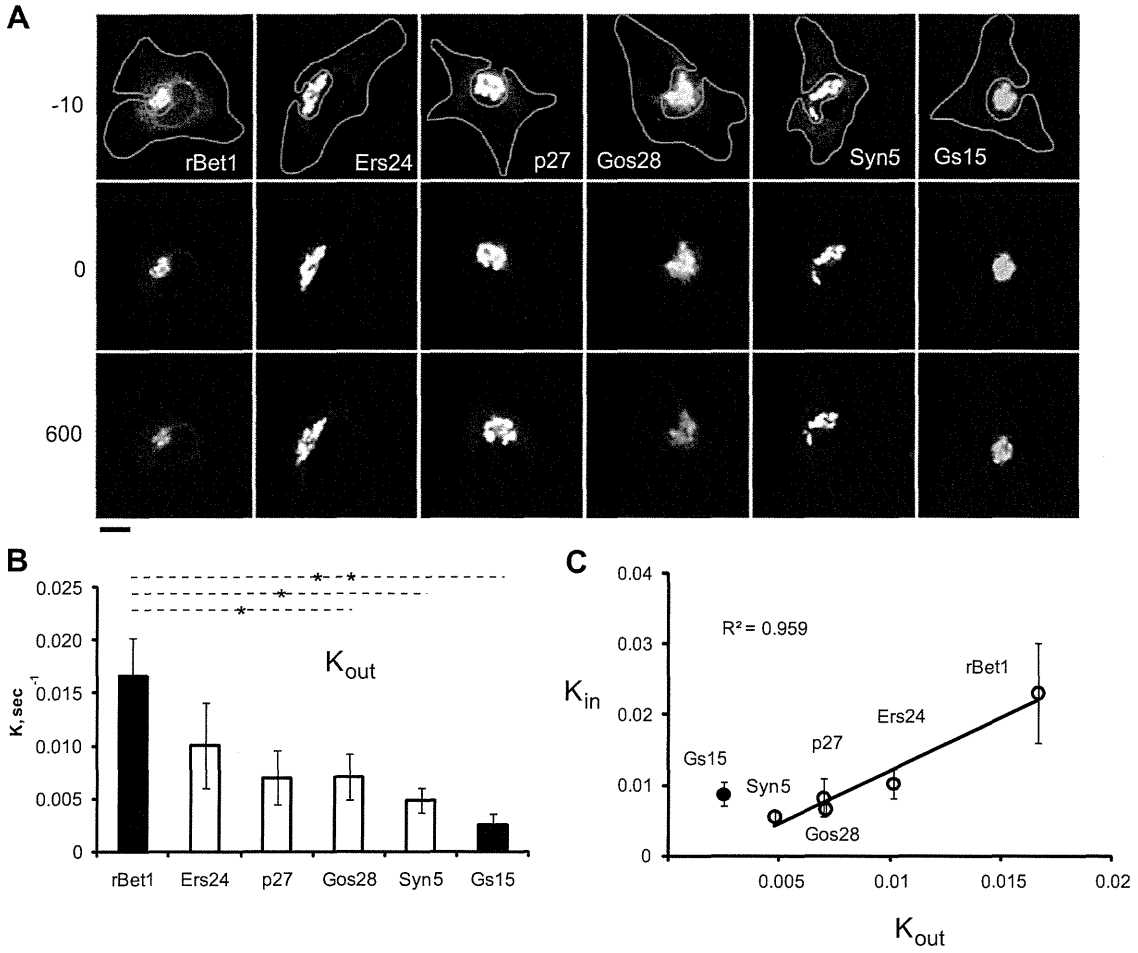

Fig. 3. Retrograde transport of SNARE proteins in the early secretory pathway. (A) CFP-tagged Golgi SNARE proteins were transiently expressed in NRK cells and retrograde transport rates were determined following the recovery of fluorescence in the ER after bleaching the ER (the regions of interest that exclude the Golgi). Representative images showing the pre-bleaching (−10 s), the post-bleaching (0 s), and the post-recovery stages (600 s) of FRAP. Scale bar = 10 μm. (B) The rates of retrograde transport of SNARE proteins. K_{out} values were calculated from single-exponential fits of fluorescence recovery curves after photobleaching the ER as described in Section 5. Bars are means ± S.E.M. for n = 10–15 cells. Statistically significant differences between K_{in} values were determined using One-way ANOVA; $^{*}P < 0.05$; $^{**}P < 0.01$. (C) Linear correlation between K_{in} (from Fig. 1D) and K_{out} (from Fig. 3B) for Golgi SNARE proteins.

anterograde–retrograde vesicular transport is involved in observed SNARE segregation in the early secretory pathway. Because the rates of anterograde and retrograde transport of SNARE proteins were similar, as expected for dynamic equilibrium, we hypothesize that SNAREs follow the constitutive recycling pathway between the Golgi and the ER. There was a linear relationship between intra-Golgi mobility rates and the rates of anterograde and retrograde transport of SNARE proteins, suggesting that the *cis*-Golgi SNAREs are more mobile in the Golgi than intra-Golgi SNAREs. Therefore we hypothesize that intra-Golgi retention controls SNARE release into the recycling pathway.

3.2. Partitioning of SNARE proteins in Golgi microdomains

It has been suggested that cholesterol concentration gradually increases from the *cis*-Golgi to the *trans*-Golgi [44]. The asymmetric distribution of cholesterol or other lipids alone the *cis*–*trans* axis of the Golgi may influence intra-Golgi mobility of SNARE proteins. The analysis of Lubrol-extracted cholesterol-containing lipid raft fractions revealed a high content of the endocytic pathway and TGN markers, including SNARE proteins Vti1 and Syntaxin 6, and non-SNARE proteins TGN38 and Rab6a (Fig. 4). In contrast, Golgi SNARE proteins showed poor partitioning or no partitioning into detergent-resistant fractions (Fig. 4). This finding was reproduced using two different cell lines. This result is consistent with a previous report that exocytic SNARE proteins Syntaxin 1 and Synaptobrevin 2 reconstituted into giant unilameller vesicles in vitro prefer the liquid-disordered phase [45]. Similar in vitro reconstitution experiments using purified Golgi SNAREs may unambiguously resolve the differences in membrane raft partitioning of *cis*-Golgi and *trans*-Golgi SNAREs in vitro.

Although protein partitioning into detergent-resistant membrane fractions is often used as the criterion for lipid raft association, this method is somewhat artificial in respect to the native state of biological membranes in vivo. While the TGN is enriched in lipid raft markers [46], the existence of intra-Golgi rafts, their composition, and the solubility in different detergents remain unknown. It is possible that differential mobility of Golgi SNARE proteins reflect the differences in membrane fluidity of individual Golgi cisternae rather than partitioning into lipid rafts. The length and amino acid composition of the transmembrane domains or differential homo and hetero oligomerization may guide SNARE proteins into different lipid domains of the Golgi membranes.

3.3. Intra-Golgi mobility of SNARE proteins and protein–protein interactions

It is now well documented that the intra-Golgi SNAREs interact genetically and physically with the Golgi tethering factors COG, GM130 and p115. These factors promote the assembly of SNARE

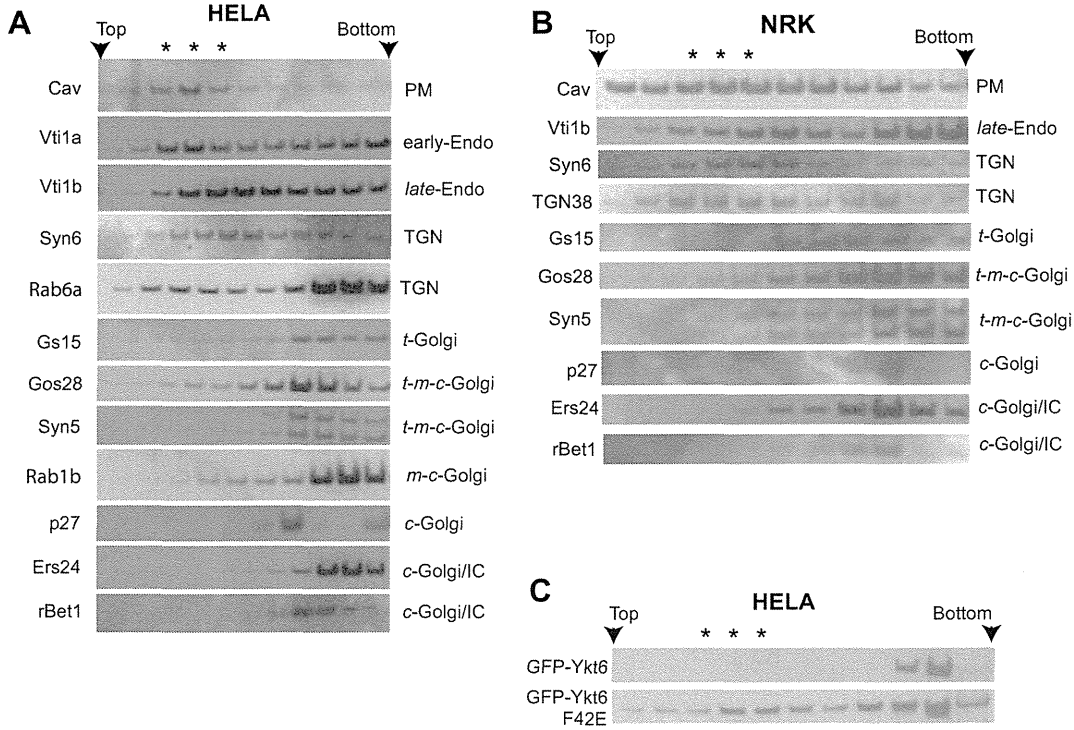

Fig. 4. SNARE partitioning in detergent-resistant membrane domains. Wild type HELA cells (A), HELA cells stably expressing GFP-Ykt6 or GFP-Ykt6-F42E (C), and wild type NRK cells (B) were lysed in the 1% Lubrol WX-containing buffer, and fractionated by sucrose density gradient ultracentrifugation as described in Section and Fig. 1S. Caveolin (Cav), Golgi SNAREs (Syntaxin5 (Syn5), p27, Ers24, rBet1, Gs15, and Gos28, GFP-tagged Ykt6s), TGN SNARE (Syntaxin6 (Syn6)), endosomal SNAREs (Vti1a and Vti1b), Rab1b, Rab6a and TGN38 levels in the resulting fractions were analyzed by immunoblot as described in Section 5. Asterisks indicate the position of Cav-containing detergent resistant rafts. PM, plasma membrane; early-Endo, early endosomes; late-Endo, late endosomes; TGN, *trans*-Golgi network; *t*-Golgi, *trans*-Golgi; *t-m-c*-Golgi, *trans, medial, cis*-Golgi compartments; IC, intermediate compartment.

complexes and localization of SNARE proteins to the Golgi (reviewed in [47]). Recent study suggests that Gos28 and Syntaxin5, but not Ers24, Bet1 and Gs15 bind the components of the COG complex in vivo [48]. This study agrees with the present report that Gos28 and Syntaxin5 have the lowest mobility, while rBet1, Ers24 and Gs15 have the highest mobility in the Golgi membranes (Fig. 5). We hypothesize that the *trans*-Golgi *t*-SNAREs *Gos28* and Syntaxin5 are stably associated with immobile fraction comprised of tethers and/or other Golgi proteins. In contrast, *v*-SNAREs rBet1 and Gs15 that don't bind the known tethers [48] have higher mobility in the Golgi (Fig. 5). The yeast homolog of the *trans*-Golgi *t*-SNAREs Ykt6 has been shown to bind the GOG complex in yeast [49], although its intra-Golgi mobility was not examined in the present study. Thus, the spatial segregation of the *cis*-Golgi and *trans*-Golgi SNAREpins correlate with their differential association with the Golgi tethering factors.

Homo and hetero oligomerization of SNARE proteins via their transmembrane or cytoplasmic domains may also contribute to their localization mechanism in the Golgi. Although numerous co-immunoprecipitation studies suggest that *trans*-SNARE complexes are relatively unabundant in the cell, one can argue that detergent solubilization may disrupt weak protein–protein interactions that bind SNARE proteins in a delicate protein network, consisting of fusogenic and inhibitory SNARE partners and Golgi tethers. These weak, possibly transient interactions may hold SNARE proteins in place and also regulate fusion specificity of membrane compartments.

3.4. Golgi localization of SNARE proteins and i-SNARE hypothesis

Although vesicle recycling and/or association with Golgi proteins or lipids may modulate the steady-state levels of SNARE proteins in the Golgi, one additional mechanism remains untested in vivo. We previously described a new functional class of SNAREs, designated inhibitory SNAREs (*i*-SNAREs) [27]. An *i*-SNARE inhibits membrane fusion by substituting for a subunit of a fusogenic SNARE complex to form a non-fusogenic complex. For example, the *cis*-Golgi SNAREs Bet1 and p27 function as the *i*-SNAREs that inhibit fusion mediated by the *trans*-Golgi SNAREs, and the *trans*-Golgi SNAREs Gs15 and Gos28 function as the *i*-SNAREs that inhibit fusion mediated by the *cis*-Golgi SNAREs [27].

This finding has two strong implications that (i) SNAREs can mediate topologically restricted membrane fusion, and (ii) SNAREs can regulate their own distribution in the Golgi stack. *i*-SNAREs may also drive the homotypic fusion of *trans*-Golgi membranes by restricting fusion of vesicles enriched in the *cis*-Golgi SNAREs with the *trans*-Golgi compartments, and by allowing fusion of vesicles enriched in the *trans*-Golgi SNAREs with the *trans*-Golgi compartments. The same rule may apply to the homotypic fusion in the *cis*-Golgi. This process may lead to formation of non-identical compartments and the apparent gradient-like distribution of SNARE proteins across the Golgi stack. Because the yeast Golgi is not assembled in a pancake-like structure of the mammalian Golgi, it is possible that homotypic assembly of Golgi compartments, in the absence of their spatial alignment, is sufficient for mediating Golgi function, including cargo sorting and protein glycosylation. The question arises as whether the inhibitor–activator relationship exists among the other classes of Golgi proteins and how the homotypic and heterotypic ensembles of SNARE proteins regulate self-organization of the Golgi.

3.5. SNARE sorting into different transport vesicles

The mechanisms, which explain the different transport rates of SNARE proteins, remain unclear. It is possible that vesicle fusion specificity (reflected by different transport rates) can be

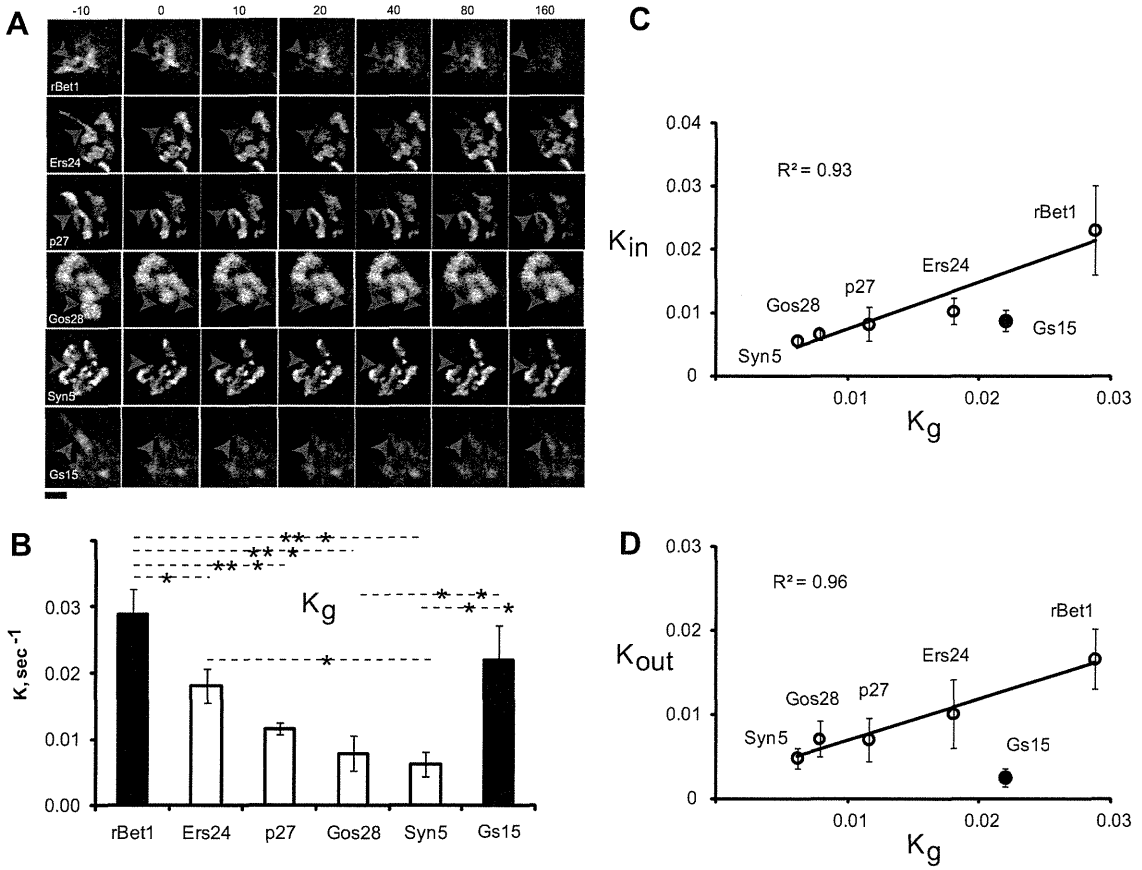

Fig. 5. Intra-Golgi mobility of SNARE proteins. (A) CFP-tagged Golgi SNARE proteins were transiently expressed in NRK cells and intra-Golgi transport rates were determined following fluorescence recovery of small photobleached Golgi regions (marked with arrowheads) as described in Section 5. The time course of fluorescence recovery is shown in seconds. B) K_g values were calculated from single-exponential fits of fluorescence recovery curves after photobleaching parts of the Golgi. Bars are means ± S.E.M. for $n = 10–15$. Statistically significant differences between K_{in} values were determined using One-way ANOVA; $^{*}P < 0.05$; $^{**}P < 0.01$; $^{***}P < 0.001$. (C) Linear correlation between K_{in} (from Fig. 1D) and K_g (from Fig. 5B) for Golgi SNARE proteins. (D) Linear correlation between K_{out} (from Fig. 3B) and K_g (from Fig. 5B) for Golgi SNARE proteins. The rates = s^{-1}.

programmed during SNARE sorting into different types of transport vesicles in the Golgi. For instance, rBet1 and GS15 may bind the *cis*-Golgi and *trans*-Golgi sets of coat proteins, respectively, guiding *cis*-Golgi and *trans*-Golgi v-SNAREs into different populations of Golgi-derived COPI vesicles [50–52]. Intra-Golgi SNAREs might enter both the *cis*-Golgi and the *trans*-Golgi types of COPI vesicles, although the third "mixed" type of COPI vesicles involved in intra-Golgi sorting of SNAREs may also exist.

A similar type of the sorting mechanism operating at the vesicle budding sites in the ER may drive the *cis*-Golgi *v*-SNARE rBet1 into a distinct (and possibly more fusogenic) type of COPII vesicles, resulting in the segregation of rBet1 from other SNAREs [53,54], explaining faster recovery rates for rBet1 in the Golgi. It is noteworthy that the *i*-SNARE-mediated mechanism might preclude undesirable fusion events between different types of vesicles by keeping a subset of SNAREs in a passive "passenger" mode.

4. Conclusions

Unfortunately, the FRAP-based method alone cannot resolve the mechanism of intra-Golgi transport of SNARE proteins. The measured transport rates in the Golgi might reflect the number of transport steps within the Golgi which may occur by several independent mechanisms, including vesicle- or tubule-mediated transport, lateral diffusion in the Golgi membranes, or cisternae maturation (reviewed in [55,56]). It is likely that a combination of these mechanisms contribute to SNARE localization. Other methods that involve super-resolution imaging and reversible inactivation of the Golgi proteins are required to unambiguously resolve the mechanisms of intra-Golgi transport of SNARE proteins [57].

5. Materials and methods

5.1. Recombinant techniques, cell culture and protein expression

The coding regions of rat Bet1, p27, and Syntaxin5, mouse Gs15, Chinese hamster Gos28 and Ers24 have been subcloned in frame into BamH1/Mlu1 sites of modified (Mlu1 site was introduced between BamH1 and Xba1) pECFP-C1 or SacII/BamH1 sites of pECFP-N1 vectors (Clontech Laboratories Inc., Mountain View USA). Similar GFP-SNARE constructs have been described [29]. NRK cells were cultured in 8-well chambers (Lab-Tek II chambered #1.5, German coverglass system, Nalge Nunc International, Rochester, NY, USA) in DMEM containing 10% fetal calf serum, penicillin, streptomycin, and fungizone (Invitrogen, Grand Island, NY, USA). Cells were transfected with 2 μg DNA using FuGENE HD transfection reagent (Promega Corporation, Madison, USA) and assayed within 24 h after transfection. Only cells expressing low levels of CFP-tagged proteins were used for analysis.

5.2. Live-cell microscopy and image analysis

Image recording was conducted using an inverted Leica SP5 AOBS spectral confocal system equipped with a motorized, temperature-controlled stage and 63x HCX PL APO (NE = 1.451)

glycerol objectives. CFP was excited with an Argon laser, and images were recorded at emission bandwidth of 500–550 nm. Photobleaching was performed using the built-in FRAP module of the Leica confocal microscope. Anterograde (K_{in}), retrograde (K_{out}), and intra-Golgi (K_g) rates of transport were calculated as follows. Raw fluorescent values obtained from the post-bleach recovery traces (F_{pb}) were background (F_b)-corrected and initial fluorescence values (F_0) were set to zero:

$$F = (F_{pb} - F_b) - (F_0 - F_b)$$

The corrected traces were used for rate (K) calculations using the single exponential fit function in GraphPad Prism, version-4 software:

$$F = F_{max}(1 - e^{-Kt})$$

The goodness of fit was determined using the R^2 values. Cells that displayed focus shift or movements during the recovery of fluorescence were not included in analysis.

5.3. Flotation of lipid raft fractions

Lipid raft fractions were separated as described previously [58] with 1% (v/v) Lubrol WX instead of Triton X-100 as a detergent. In brief, sub-confluent HeLa cells in two 10 cm-dishes, after being washed with PBS, were harvested by scraping and precipitated by centrifugation at 300×*g* for 5 min. The precipitated cells were extracted with 100 μl of 1% (v/v) Lubrol WX in MN buffer (25 mM MES-NaOH, pH 6.5) containing 0.15 M NaCl and a protease inhibitor cocktail (Complete™ EDTA-free, Roche) for 30 min on ice. Cell extracts were diluted into 500 μl, by adding 85% (w/v) sucrose in MN buffer, and layered under 8 ml of a 10–30% sucrose gradient in MN buffer. After centrifugation at 75000×*g* for 20 h at 4 °C, 0.75-ml fractions were collected from the top of the resulting gradient.

5.4. Antibodies

Rabbit polyclonal antibody against Caveolin was purchased from Santa Cruz Biotechnology. Mouse monoclonal antibodies against Vti1a and Vti1b were from BD Biosciences, against rBet1 (clone 16G6) from StressGen Biotechnology, and against GFP from Roche Applied Science. Mouse monoclonal antibodies against Rab1b (clone M1E7) and Rab6a (clone 5B10) were gifted from T. Mayer [59]. Rabbit polyclonal antibodies against Gos28, Syntaxin5, Ers24, p27, Syntaxin 6, and Gs15 were generated and affinity-purified as described previously [60].

5.5. Immunoblot analysis

Each fraction was solubilized with NuPAGE LDS sample buffer (Invitrogen) containing 50 mM DTT and then heated at 95 °C for 5 min. Electrophoresis of these samples was performed in precast NuPAGE 10% or 12% bis–tris gels (Invitrogen). For immunoblot analysis, the proteins were transferred to polyvinylidene difluoride membranes (Invitrogen), and the blotted membrane was incubated with primary antibodies, at a 1:1000 dilution, for 90 min. Horseradish peroxidase-conjugated secondary antibody (GE healthcare), at a 1:1000 dilution, was incubated with the blot for 90 min. Detection was performed by using ECL (GE Healthcare) and fluorography.

5.6. Cell culture and establishment of GFP-tagged Ykt6-expressing cells

All cells were grown in Dulbecco's modified Eagle's medium (DMEM) supplemented with 10% fetal bovine serum (FBS), 100 U/ml Penicillin G, and 100 mg/ml streptomycin sulfate under a 5% CO_2 atmosphere at 37 °C. Mammalian expression vectors of GFP-tagged Ykt6 and Ykt6-F42E were constructed as described previously [40]. To establish cells stably expressing GFP-Ykt6 or GFP-Ykt6-F42E, HeLa cells were transfected with these plasmids using FuGENE 6 Transfection Reagent (Roche), selected by G418 resistance, and cloned. Exogenous Ykt6 expression in these cell clones was confirmed by fluorescent microscopy.

5.7. Permeabilized cell assay

NRK cells were permeabilized as described [61]. Briefly, cells were rinsed with cold KHM buffer (25 mM HEPES pH 7.4, 125 mM potassium acetate, 2.5 mM magnesium acetate), and incubated for 10 min on ice in the presence of 30 μg/ml digitonin (Calbiochem) in KHM buffer. In NSF rescue experiments, 0.2 mM NEM was added to a permeabilazation mixture. NEM was neutralized by 0.4 mM DTT for 5 min. Cells were rinsed with cold KHM buffer, and then incubated for 10–20 min on ice in 200 μl transport mixture (5 mM ATP, ATP-regenerating system, 50% bovine brain cytosol, KHM buffer, 5–10 μg NSF and 5–10 μg alpha-SNAP). Recombinant Sar1 mutant (Sar1 T39N) was purified as described [62] and dialyzed against KHM buffer containing 10 μM GDP and 0.5 mM DTT. Ten to twenty micrograms of Sar1 T39N was added to a transport mixture.

Appendix A. Supplementary data

Supplementary data associated with this article can be found, in the online version, at http://dx.doi.org/10.1016/j.febslet.2013.06.004.

References

[1] Rothman, J.E. and Wieland, F.T. (1996) Protein sorting by transport vesicles. Science 272, 227–234.
[2] Lippincott-Schwartz, J., Yuan, L.C., Bonifacino, J.S. and Klausner, R.D. (1989) Rapid redistribution of Golgi proteins into the ER in cells treated with brefeldin A: evidence for membrane cycling from Golgi to ER. Cell 56, 801–813.
[3] Dean, N. and Pelham, H.R. (1990) Recycling of proteins from the Golgi compartment to the ER in yeast. J. Cell Biol. 111, 369–377.
[4] Lewis, M.J. and Pelham, H.R. (1992) Ligand-induced redistribution of a human KDEL receptor from the Golgi complex to the endoplasmic reticulum. Cell 68, 353–364.
[5] Hammond, C. and Helenius, A. (1994) Quality control in the secretory pathway: retention of a misfolded viral membrane glycoprotein involves cycling between the ER, intermediate compartment, and Golgi apparatus. J. Cell Biol. 126, 41–52.
[6] Scales, S.J., Pepperkok, R. and Kreis, T.E. (1997) Visualization of ER-to-Golgi transport in living cells reveals a sequential mode of action for COPII and COPI. Cell 90, 1137–1148.
[7] Cole, N.B., Ellenberg, J., Song, J., DiEuliis, D. and Lippincott-Schwartz, J. (1998) Retrograde transport of Golgi-localized proteins to the ER. J. Cell Biol. 140, 1–15.
[8] Storrie, B., White, J., Rottger, S., Stelzer, E.H., Suganuma, T. and Nilsson, T. (1998) Recycling of golgi-resident glycosyltransferases through the ER reveals a novel pathway and provides an explanation for nocodazole-induced Golgi scattering. J. Cell Biol. 143, 1505–1521.
[9] Todorow, Z., Spang, A., Carmack, E., Yates, J. and Schekman, R. (2000) Active recycling of yeast Golgi mannosyltransferase complexes through the endoplasmic reticulum. Proc. Natl. Acad. Sci. USA 97, 13643–13648.
[10] Sollner, T., Whiteheart, S.W., Brunner, M., Erdjument-Bromage, H., Geromanos, S., Tempst, P. and Rothman, J.E. (1993) SNAP receptors implicated in vesicle targeting and fusion. Nature 362, 318–324.
[11] Newman, A.P. and Ferro-Novick, S. (1987) Characterization of new mutants in the early part of the yeast secretory pathway isolated by a [3H]mannose suicide selection. J. Cell Biol. 105, 1587–1594.
[12] Hay, J.C., Hirling, H. and Scheller, R.H. (1996) Mammalian vesicle trafficking proteins of the endoplasmic reticulum and Golgi apparatus. J. Biol. Chem. 271, 5671–5679.
[13] Kaiser, C.A. and Schekman, R. (1990) Distinct sets of SEC genes govern transport vesicle formation and fusion early in the secretory pathway. Cell 61, 723–733.